University of Bath

Alternative formats

If you require this document in an alternative format, please contact:
openaccess@bath.ac.uk

Silk-based Biopolymers Promise Extensive Biomedical Applications in Tissue engineering, Drug Delivery, and BioMEMS

Amirhossein Farahani [a,*], Abbas Zarei-Hanzaki [b,*], Hamid Reza Abedi [c], Sara Daryoush [d], Fatemeh Mianabadi [e], Sahar Shahparvar [b], Mohammad Akrami [f], Ebrahim Mostafavi[g, h], Hamideh Khanbareh [i], Farhad R. Nezami [j]

[a] Department of Engineering Science and Mechanics, Penn State, USA

[b] Hot Deformation & Thermomechanical Processing Laboratory of High Performance Engineering Materials, School of Metallurgy and Materials Engineering, College of Engineering, University of Tehran, Tehran, Iran.

[c] School of Metallurgy & Materials Engineering, Iran University of Science and Technology (IUST), Tehran, Iran

[d] Department of Chemical Engineering, The Pennsylvania State University, University Park, PA, 16802, USA

[e] Department of Petroleum and Chemical Engineering, Sharif University of Technology, Tehran, Iran

[f] Department of Pharmaceutical Biomaterials, and Medical Biomaterials Research Center, Faculty of Pharmacy, Tehran University of Medical Sciences, Tehran, Iran.

[g] Stanford Cardiovascular Institute, Stanford University School of Medicine, Stanford, CA 94305, USA

[h] Department of Medicine, Stanford University School of Medicine, Stanford, CA 94305, USA

[i] Department of Mechanical Engineering, University of Bath, Claverton Down, Bath BA2 7AY, UK

[j] Division of Thoracic and Cardiac Surgery, Brigham and Women's Hospital, Harvard Medical School, Boston, MA 02115, USA

Abstract

As an FDA-approved biopolymer, Silk has been contemplated for a wide range of applications based on its unique merits, such as biocompatibility, biodegradability, and piezoelectricity. As Silk, in both crystalline structure and amorphous state, exhibits unique physical, mechanical and biological properties (promoting cell migration, differentiation, growth, and protein-surface interaction), it is fruitful to understand its potential applications. Sensors, actuators, and drug delivery systems are the best in case. As such, the current effort first introduces Silk Fibroin (SF) and delineates its characteristics. It then explores the extensive use of this biomaterial in tissue engineering approaches, in addition to its biosensor and electro-active wearable bioelectronic application. To this end, the SF application in cardiovascular, skin, cartilage, and drug delivery systems for cancer therapy and wound healing were studied precisely. Compositing any type of other variables to induce a specific application or improve any SF barriers, namely its hydrophobicity, poor electrical conductivity, or tuning its mechanical properties, especially in tissue engineering application, has also been discussed wherever it deemed informative.

1. Introduction

As an advantageous natural biopolymer, silk fibroin (SF) is constructed from a group of proteins originated from silkworms and spiders. Silk consists of fibroin (Crystalline structure) and an amorphous protein called Sericin; As a semicrystalline polymer, Silk's crystalline regions are comprised of β-sheet blocks. Any changes in Silk's β-sheet crystalline regions' content due to the chemo-physical or heat treatment process would cause meaningful alterations in chemical, physical, mechanical, and biological properties; various research groups have focused on studying the effect of these alternations [1].

Silk, as an auspicious FDA-approved biomaterial, is a profitable substrate for tissue engineering applications due to its biocompatibility, biodegradability, and hemocompatibility, as well as bio-resorbability. Sericin's impact on biocompatibility depends on the application. Several investigations have established a further benefit of using Silk sericin for wound healing considerations. Jiao et al. [2] demonstrated that Sericin not only did not trigger an allergenic response but also exhibited low and adequate immunogenicity. On the other hand, there has been several reports of immune responses to Silk sutures containing Sericin proteins. Therefore, degumming is a typical strategy to sidestep probable inflammation in tissue engineering applications [3].

Silk's tissue engineering application can be classified into two differentiated areas– hard and soft tissue engineering. However, this study considers its soft tissue engineering application

in cardiac, vascular, skin, and cartilage tissue engineering systems, to name but a few. There are multiple methodologies to synthesis silk mats for soft tissue engineering application with different requirements such as porosity and natural tissue matrix's mimicking, that should be considered to support the cultivated cells. As such, 3D printing is the most recently suggested approach to reach the exact tissue mimetic scaffold [4]. At the same time, the electrospinning method forms micro/nanofibrous platforms affecting the microstructure of the fibers [5]. Additionally, freeze-drying provokes a highly porous structure, encouraging the cells to migrate and reconstruct the damaged tissue [6].

Besides, Silk as a natural protein has been considered an advantageous biomaterial for developing drug delivery systems [7]. It has suitable chemical and biological properties for sustainable drug delivery approaches, including bio-compatibility, bio-degradability, non-toxic by-products, mild aqueous processing to maintain bioactive features of the drug, and versatility of options for sterilization. In addition, the mechanical stability and self-assembly properties of the SF lead to a slow degradation rate, wherein a controlled drug release kinetics and near zero-order sustained release behavior can be achieved through diffusion- and degradation-driven mechanisms [8].

Furthermore, multiple methods are considered to attain various SF delivery system applications, such as microspheres, nanoparticles, hydrogels, films, nanofibers, lyophilized sponges, and SF-coated polymeric particles. Because of the looked-for properties, silk-based materials have an extraordinary demand to be used in the pharmaceutical industry to produce sustained drug delivery systems [9]. Silk as a natural protein has been considered as an advantageous biomaterial for developing drug delivery systems (DDSs) [7]. Sericin, a glue-like protein, may trigger an immunogenic reaction by getting wrapped around the SF. Sericin is divided

3

from the SF by a process recognized as degumming [10]. Hereunder, the current status of Silk biomaterials' prospective administration in cancer treatment and wound healing applications are considered.

At the final stage, this paper considers Silk's piezoelectric application. As described in the literature [11], the non-centrosymmetric structure of the Silk would cause it to have electro-active properties. Thus, applying mechanical deformation into the samples generates electrical potential in them and vice versa [12]. This intellectual property renders Silk an exciting material for biosensing, BioMEMS, and wearable bioelectronic applications discussed in the following sections.

2. Chemistry-structural evolution effect on physical properties

The raw SF, forming a Bombyx mori cocoon, comprises of a semicrystalline protein called fibroin and an amorphous protein called Sericin, wherein the amorphous parts function as a gumming agent [13,14]. It has been reported that sericin-free unprocessed fibroin fiber shows a better mechanical property [15]. New investigations has also demonstrated that Sericin could boost the mechanical properties of processed (freeze-dried) Silk without cytotoxicity effect [16].

SF is a high-molecular-weight block copolymer which is consisted of heavy (≈ 370 kDa) and light (≈ 26 kDa) chains; the hydrophobic stable anti-parallel β-sheet crystalline blocks are linked by small hydrophilic linker segments or spacers [17]. A semicrystalline structure can be obtained from SF regeneration process which has consisted of three types of crystalline regions. Silk I or silk II are Equilibrium-stable phases, while the unstable Silk III can be characterized at the air/water interface. The amorphous state of semicrystalline Silk consists of α-helices, turns, and random coil structures [18].

Moreover, SF has a crystalline polymorphism structure. Silk 1 follows a metastable structure with helical and less-extended conformation that usually transforms to silk 2, with a monoclinic unit cell. In contrast, its protein chains are pleated as β-sheet (two-fold "zig-zag") conformation [19]. The transformation from Silk I to silk II occurs by shear or Methanol/Potassium-phosphate treatment [14]. Silk III structure contributes a trigonal symmetry, suggesting a left-handed three-folded helical structure of polyglycine-2 conformation for the Silk chains. It has been demonstrated that SF structure and various conformations cause a lack of symmetry center in all its available forms, where the source of the piezoelectricity is demonstrated to be rooted in the non-centrosymmetric structures [11]. Fukada et al [20] quantified the intrinsic shear piezoelectricity of SF bundles and calculated a d_{14} piezoelectric constant around of 1 pC/N, comparable to that of the quartz crystal (≈2 pC/N).

The piezoelectricity of the Silk is principally recognized by the net-polarization of the uniaxially aligned Silk II crystals perpendicular to the plane of the applied shear force. As such, silk piezoelectricity depends on a combination of high β-sheet crystal content and crystal orientation; thus, the promotion of the crystalline content results in piezoelectricity improvement [21]. Different methods such as ethanol or methanol treatment, mechanical stretching, and subsequent heat/cooling treatments have been utilized to increase β–sheet fraction so as to enhance the silk piezoelectricity [22].

Additionally, the existence of β-sheet imparts protein-based material with high mechanical strength and toughness. Conferring to the literature, degummed Silk has improved strength and toughness compared to other degradable polymers [17]. It's worth mentioning that in tissue engineering (TE), scaffolds are made from regenerative Silk and the differences between the two SF types has been shown in numerous studies [23]. Degummed silk is readily assembled into

hierarchical structures with an impressive tensile strength, but the hierarchical structure of regenerated one is disrupted, which deteriorates the mechanical properties and affects the degradation. The degradation rate of SF varies from days to several months, depending on the employed processing method that specifically breaks down the protein chains, and causes structural conformation change of the crystalline regions [24]. SF is responsive to enzymes, such as α-chymotrypsin, protease XIV, and collagenase IA, and can degrade by them. Varying fabrication techniques can lead to a broad range of structural, mechanical, and biological characteristics that may also affect the degradation process [14,25,26].

3. Tissue Engineering application

Silk fibers are assuring biomaterials in TE as they contain all the enquired properties such as ease of mechanical properties tunability, degradability, composition, and sequences. Several research groups have reported that SF nets are highly human-cell compatible and potentially useful as a new scaffolding substrate for a wide range of intended tissues [27]. Rnjak-Kovacina showed that by varying β-sheet's concentrations, suitable properties could be achieved [28]. In addition, tunable stiffness and ECM mimetic microstructures would be reached by regulating the amorphization rate. As a result, it adjusts cell proliferation directly and promotes in vivo neovascularization [29].

Considering the inherent Silk features [30], piezoelectricity for instance, new bio-applications would be flaunted, and promising approaches for them will be developed. It has been discovered that the body has some bioelectric signals, and electrical stimulation hypothetically promotes cell growth, proliferation, and tissue regeneration [31]. Since piezoelectric materials can generate voltage and provide electrical stimulation without electrodes or an external power source, bio-piezoelectric materials should be promising to apply such electrical stimulation to the tissues.

It has recently been verified that SF/PVDF composite has piezoelectric characteristics, and an augmentation of cell proliferation in piezoelectric PVDF/SF patches was observed (Fig.1(a)), which has the potential to be investigated and considered more accurately [22].
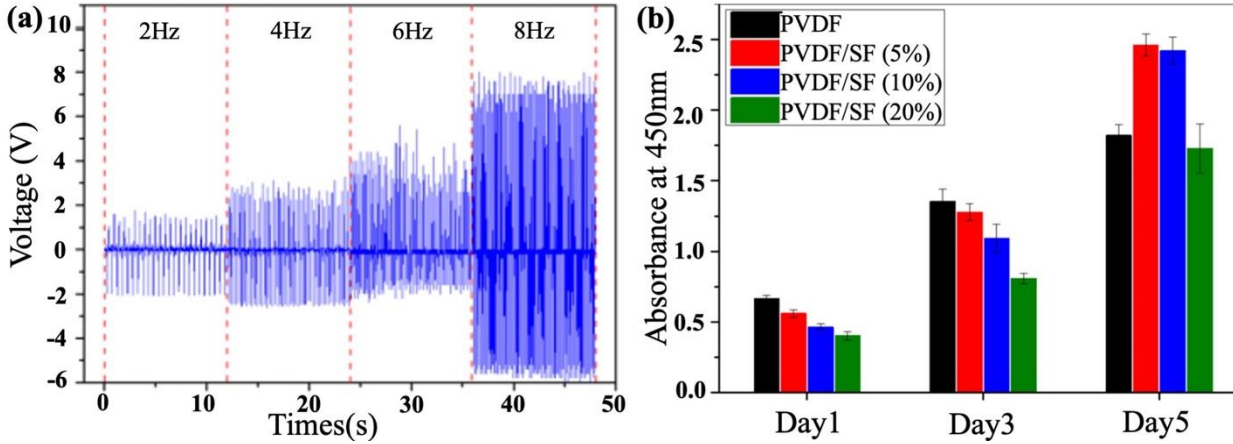

Fig.1 (a) Output voltage of electrospun Polyvinylidene fluoride (PVDF)/ Silk fibroin (SF) (Placeholder1)(10%). (b) Analysis of cell proliferation (CCK-8 assay) on the surface of electrospun fiber was manufactured by adjusting the content of SF (5%, 10%, and 20%) based on the weight of PVDF after incubation for 1, 3, and 5 days [22].

Numerous reports have illustrated that how different fabrication methods, such as blending, compositing, cross-linking, etc., can be used to achieve the most appropriate properties of the scaffolds regarding the particular usage in TE [13,25,32].

3.1 Cardiac Tissue Engineering

Cardiovascular diseases are recognized as the leading cause of death worldwide. Loss of purposeful irreplaceable cardiomyocytes is the primary origin of mortality. Cardiac TE (CTE) has been recognized as a promising solution to refine cardiac functions [33]. In CTE, synchronous beating due to aligned sarcomeres and electrical coupling is essential for cardiomyocytes' efficient attachment. Recently synthesized non-mulberry Tasar Silk fibroin lyophilized scaffold has aligned sarcomeres growth, cell-to-cell communication, and synchronous contractions [34]. The functional

activity of cardiomyocytes is a crucial aspect of CTE, wherein the addition of carbon quantum dots (bioactive agents) into the SF/PLA nanofibrous patches increases the metabolic activity and viability of the cardiomyocytes [35].

The possible procedures to adjust scaffolds' electrical conductivity and mechanical properties remain as a challenge with its vital role in CTE. It was indicated that the assimilation of 2D nanosheets like molybdenum disulfide (MoS2) and Reduced Graphene Oxide (rGO) to Silk boosts its electrical conductivity and mechanical properties. In addition, Silk/rGO and Silk/MoS2 nanofibrous scaffold presented improved cell attachment, elongated morphology, and cell proliferation [36].

Recently it has been reported [37] that polypyrrole (PPy) encapsulated SF electrospun scaffolds can more realistically mimic the ECM due to doped PPy reduced fiber diameter. The scaffold's electrical conductivity intensifies by increasing the PPy-SF ratio to 70:30, while electrospinning is as well affected by solution conductivity. Higher conductivity causes a stronger electrostatic force that stretches the fiber (Fig.2).The Silk/PPy (7%/15%) mat supported the Neonatal rat cardiomyocyte alignment, enhanced cardiac-specific protein expression, promoted cell-cell couplings, and induced muscular injury contractions. Electrical stimulation frequently increased the displacement of the mat and the beating , and also improved the cell alignment and contraction synchrony making it a suitable electroactive scaffold for cardiomyogenesis [38].
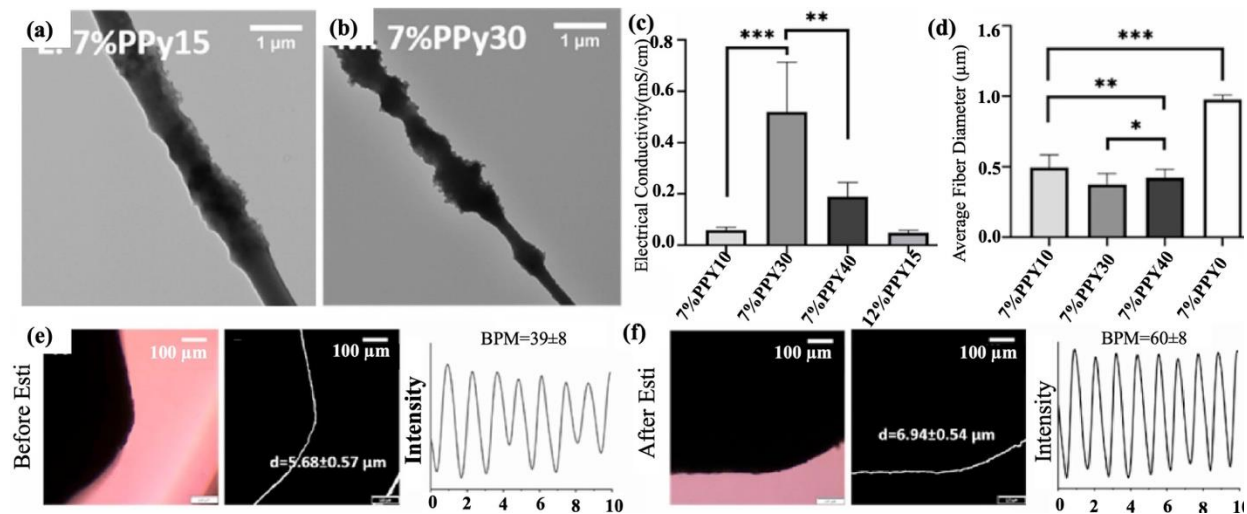
Fig.2 Morphology of ES (PPy, SF) Mats made of 7%SF with the PPy-to-SF ratio of (a) 15:85 (b) 30:70, (c) electrical conductivity (n = 3) of ES (PPy, SF) mats with different PPy-to-SF ratios. (d) Average fiber diameter of ES (PPy, SF) mats with different SF contents but identical PPy-to-SF ratio (15:85) electrical conductivity (n = 3) of ES (PPy, SF) mats with different PPy-to-SF ratios. (e-f) Phenotypes of NRCMs on ES (PPy, SF) Mats before and after Electrical Stimulation. Microscope observation, stacked photo sequence of the processed contraction video, and contraction cycles of NRCM-seeded 7%PPy15 (e) before and (f) after electrical stimulation p-value less than 0.05was considered significant, where *p<0.05, **P<0.01, ***P<0.001[38].

3.2 Vascular Tissue engineering

With extensive application of SF scaffolds in vascular TE, Kaplan demonstrated a promising interaction between the vascular cells and electrospun SF mats [39] highlighting the need to alter the silk hemocompatibility. Heparinized Silk as a dual-functional material showed an amendment in hemocompatibility level and controlled the growth factor release [40]. Other restrictions in engineering artificial small-diameter tissues, such as vascular scaffolds, are weak confluent endothelium on the lumenal surface, thrombus formation via platelet adhesion, and aggregation. Two different approaches have recently resolved this problem [41,42]. It was shown that enhancing anticoagulant activity expands the chance of successful vascular reconstruction,

and more anticoagulant sulfated silk scaffolds display a stronger cell attachment and better proliferation [41].

Three-dimensional (3D) scaffolds that imitate the natural extra-cellular matrix (ECM) might decrease thrombus and facilitate tissue maturation. In contrast to 3D fabricated scaffolds, freeze-dried patches presented a microporous and sponge-like structure. Endothelial cells (ECs) are well attached to the surface of the 3D microsphere-nanofibers (Fig.2(a)). After all, an upsurge in cell density after 7days indicates its biocompatibility, in comparison, the surfaces of the freeze-dried scaffolds presented less cell number than the 3D microsphere-nanofiber SF scaffolds [42]. The deployment of Electrosprayed microparticles in vascular scaffolds was introduced in PLGA/SF composites, which as well showed a significantly promoted cell attachment and proliferation [43]. Numerous studies about the influence of surface roughness on cell attachment and infiltration show that it is still a controversial issue [44,45]. As discussed previously, nano and microparticles intensify the roughness of fibers, which would modulate the cell attachment under the influence of increased roughness.
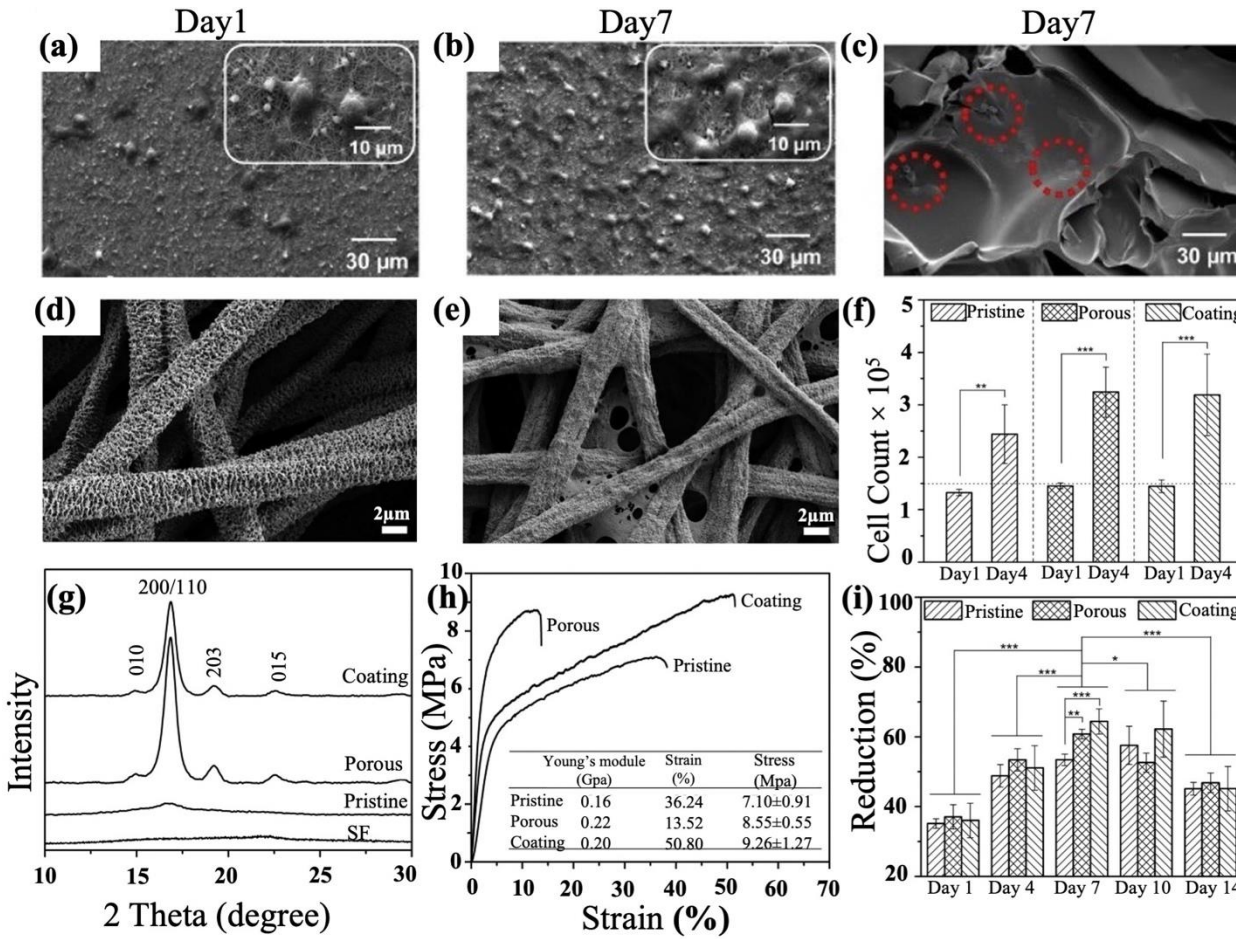
Fig.3 (a) The Scanning Electron Microscopy (SEM) micrographs of 3D microsphere-nanofiber scaffolds on Day 1, and (b) Day 7 with low magnification and high magnification in the inset micrographs. (c) SEM micrographs of ECs on freeze-dried scaffolds with a pore size of more than 150 μm. ECs in the red dash circles were observed on day 7. Scale bars = 30 μm [42]. (d) SEM of porous Poly(L-lactide) (PLLA) fibers; and (e) porous PLLA fibers with Silk Fibroin (SF) coating. (f) Cell number count on day 1 and day 4 post-seeding; and (i) Alamar blue assay results during the course of cell culture up to day 14 post-seeding. (g) X-ray diffraction analysis (XRD)spectra; (h) tensile stress-strain curves of pristine PLLA fibers, porous PLLA fibers without and with SF coating [46].

Fig.4 Schematic of (a) Fabrication of Poly (ʟ-lactide-co-ε-caprolactone) (PCLC)/ Collagen (COL) axially aligned fibers (inner layer) via customized rotating collector; (b) Fabrication of the Poly Lactic-co-Glycolic Acid (PLGA) /Silk Fibroin (SF) yarns by customized electrospinning equipment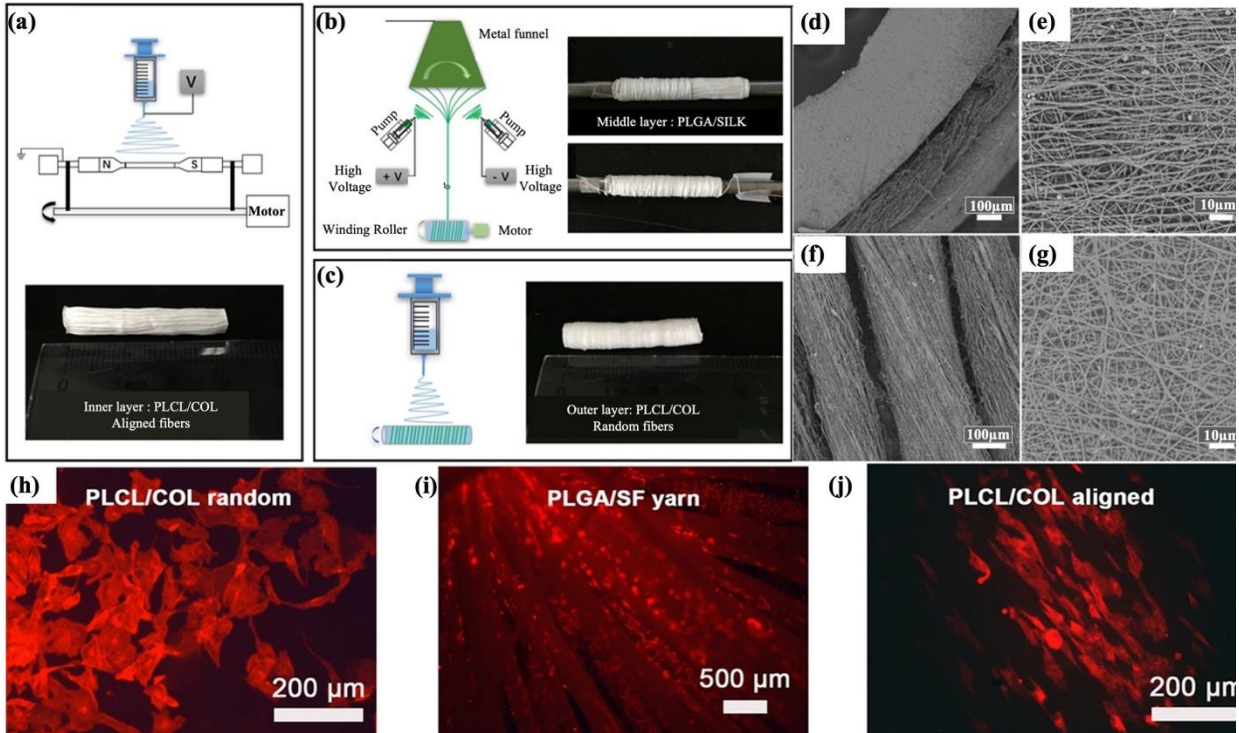. (c) Fabrication of a thin layer of PLCL/COL random fibers. SEM images showing the morphology of (d) the cross-section of the tri-layer tubular graft, (e) the aligned PLCL/COL fibers in the inner layer, (f) the PLGA/SF yarns in the middle layer, and (g) the random PLCL/COL fibers in the outer layer. The fluorescence images of HUVECs growth morphologies on (h) PLCL/COL random fibers,(i) PLCL/COL yarn, and (j) PLGA/SF aligned fibers after incubating for 3 days [47].

Another strategy to improve cell proliferation and metabolic effects is to combine SF with porous Poly-L-lactic acid (PLLA) nanofibrous materials. SF coated into prefabricated acetone treated electrospun PLLA fibers with desired porosity and mechanical properties is an alternative procedure for electrospun PLLA patches. Morphology of porous PLLA substrates and SF coated scaffold is conventionally explored via SEM images (Fig.3(d, e)). Nanoporous structure with a high specific surface area would serve as an excellent substrate to support SF. As X-ray diffraction (XRD) results show in Fig.3(g), the PLLA Electrospun patches form an amorphous structure due

to the fast solvent evaporation and low chain arrangement. SF showed almost no peaks, although it had some β-sheets due to ethanol treatment, and its crystalline peak was somewhat covered by coating porous PLLA with SF. [46].

The fluctuation of PLLA/Silk composites mechanical properties is apparent in Fig.3(h); clearly, acetone treatment decreases the elongation of the scaffold while the pores get fulfilled and covered with SF, the elongation of the fibrous membranes are significantly improved. Meanwhile, it preserved suitable Young's modules. In vitro cell culture with the smooth muscle cells after 14 days revealed that the coating of SF onto porous PLLA fibrous membranes significantly enhances cell adhesion and proliferation. It is worth mentioning that increasing the surface roughness upholds the penetrability of the scaffolds, which is an essential factor providing a greater culture medium [46].

Modifying the mechanical properties of SF was established in various attempts with different approaches such as blending, compositing, and coating. Polycaprolactone (PCL) is one of the most commonly synthesized polymers blended with SF; Xin Liu synthesized electrospun SF/PCL composite scaffolds with remarkable mechanical properties and sluggish degradability that could serve as a potential long-distance arterial vascular injury treatment material [48]. It has been reported that PLA/SF blend and PLA/Silk-fibroin-gelatin scaffolds follow an excellent toughness and flexibility and provide an ideal milieu for cell growth and proliferation [49,50]. Kuihua Zhang recommends that SF blended P(LLA-CL) nanofibrous scaffolds is a prospective vascular TE candidate [51].

Imitating the natural tissue milieu is a critical feature in TE. Multi-layered scaffolds can easily mimic the structure and purpose of natural blood vessels. The tri-layer vascular graft consisted of axially aligned Poly(L-lactide-co-caprolactone)/collagen with circumferentially

13

oriented Poly(lactide-co-glycolide)/silk synthesized by electrospinning. Innovative spinning methods and morphology of each layer have been presented in Fig.4(a-g). It is noticeable that the cells have a morphology alike to natural vessel cells. The inner aligned layer with prearranged endothelium morphology in the lumen and middle circumferential yarns regulated SMCs organization along with the single yarns, wherein the outside random fiber was fixed Fig.4(h-j) [47].

3.3 Skin Tissue engineering

Skin is the largest, principal human organ that act as a defensive barrier against several hazardous factors such as dust, opportunistic microbial, and viral infections [52]. TE is a promising method to create tissue substitutes for wounded skin. Luangbudnark et al. illustrated that blending chitosan with Silk hypothetically shifts the thermal degradation of the film due to β-sheet increment. On the other hand, chitosan augments the flexibility of the patches, which is one of the crucial descriptions of skin patches [53]. Lei et al. stated that blending Silk with PHBV (Polyhydroxybutyrate-co-hydroxy valerate) in a 50/50 ratio improves the water-uptake capability, which is a factor to store growth factors and provide compressive characteristics of the tissue [54].

Wettability is a critical characteristic of polymers that can mark cellular adhesion, proliferation, and migration. Wettability is interconnected with hydrophobicity; it has been repeatedly reported that extraordinarily hydrophilic or extremely hydrophobic surfaces prevent cell adhesion, and a moderated hydrophilic/hydrophobic surface is favored. Keirouz et al. synthesized trinary PCL-backbone SF:PGS blend composite with nozzle–free electrospinning as schematically illustrated in Fig.5(a). Reducing the contact angle by blending natural polymers and other hydrophobic polymers is currently a subject of research. Fig.5 presents the results of such attempts to improve the fibers' hydrophobicity. Trinary composite has less contact angle than PCL backbone, and by increasing SF concentration, the hydrophobicity increases. SEM images

14

presented in Fig.5(e) establish well in vitro fibroblast attachment and growth due to the addition of Silk, and this scaffold can be used in skin TE [55].

Skin wounds are highly vulnerable to microbial attack; overcoming this challenge, Acharya et al. suggested that the non-mulberry Tasar Silk is stronger and more hydrophobic compared to silk fibroin [56]. In addition, Silver nanoparticles are suitable antimicrobial replacements. Furthermore, Srivastava synthesized a Tasar nanofibrous mat coated by silver nanoparticles (AgNPs) in situ using dandelion leaf extraction that expresses excellent antimicrobial potential [57].

Crosslinking improves the mechanical properties and affects the water stability circumstances, which are essential characteristics in skin TE. An eco-friendly electrospinning process prepared GMA-modified SF Ultrathin Fibers (SF-GMA UFs). Bin Bae et al. reported that SF-GMA UFs dual cross-linking, physical and chemical, improves water solubility compared to non-crosslinked SF-GMA UFs and delivers superior cell attachment, migration, and proliferation [58]. Another significant parameter in skin architecture is its capability to support Fibroblast cell growth. Most recently, Singh Shera et al. demonstrated that Xanthan/silk blended with a 20/80 ratio, with optimized porosity and surface roughness, has a grander potential for the growth and proliferation of fibroblastic cells [59].
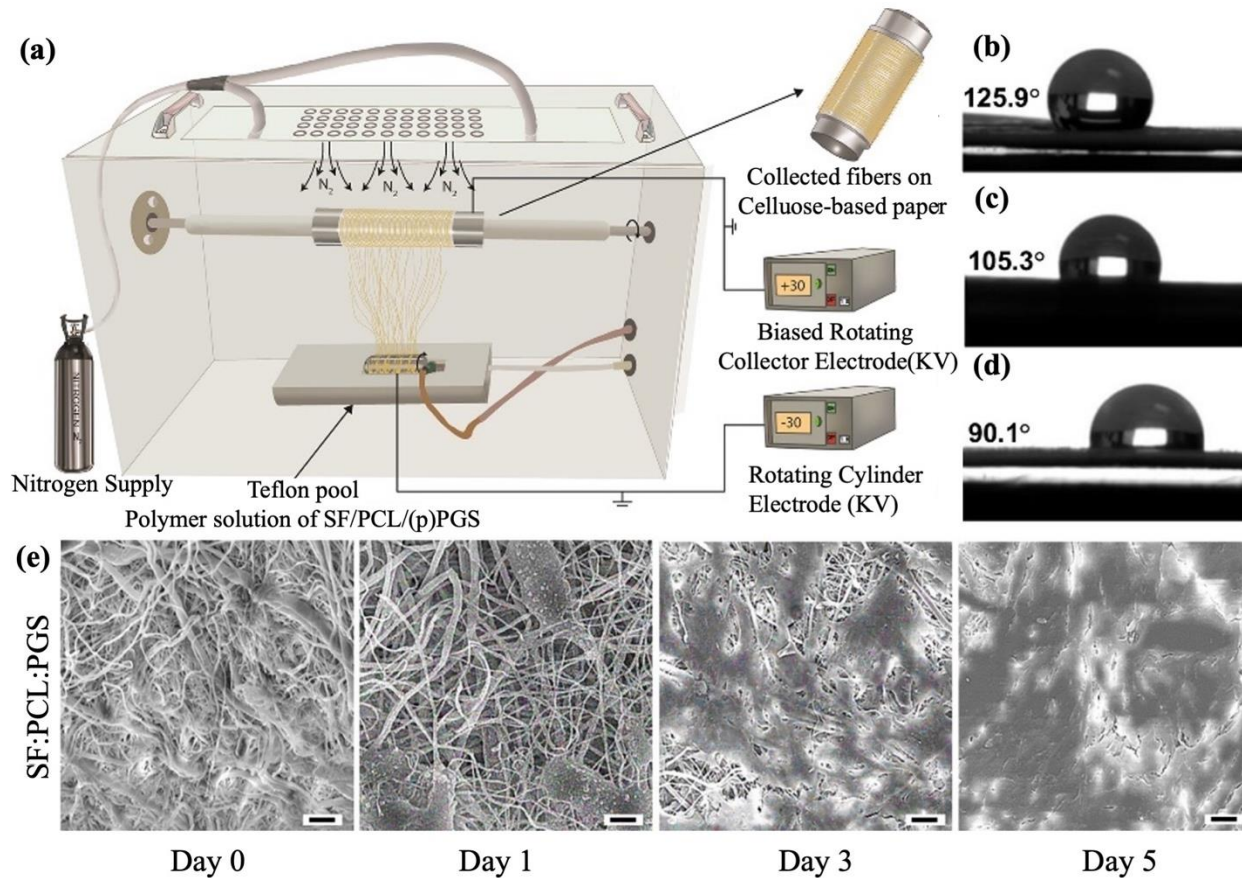
Fig.5 (a) Schematic representation of the nozzle-free electrospinning process, Water contact angle of (b) poly(ε-caprolactone) (PCL) (c) PCL-backbone Silk Fibroin (SF): Poly(Glycerol Sebacate) (PGS) ratio 1:0.75:0.25, (b) 1:0.50:0.50 (e) SEM images of HDF-TERT seeded morphology on the trinary SF:PCL:PGS 1:0.5:0.5 electrospun scaffolds. Scale bar is 10 μm [55].

3.4 Cartilage Tissue engineering

Cartilage is a flexible connective tissue with several functions, reducing friction between joints, holding bones together, and supporting other tissues; to name but a few [60]. Cartilage is composed of chondrocytes embedded within an extracellular matrix (ECM) consisting of collagen type II (60%), proteoglycans (25%), and glycoproteins (15%). The matrix is secreted by chondrocytes, providing integrin–ligand interactions and mechanical support for cells and tissue [61].

Due to the cartilage matrix's avascular, aneural, and lymphatic nature, it has a limited capacity for self-regeneration after injury. Furthermore, chondrocytes surrounded by ECM can't freely migrate to the site of injury, which leads to slow deposition of new matrix [62]. Damaged articular cartilage causes severe pain, inflammation, and some degree of disability. Current cartilage defect treatment methods include drilling, autologous chondrocyte implantation (ACI), and osteochondral allograft [63]. Though these contemporary treatment methods reduce pain and increase mobility, they are associated with major limitations such as healing complications of the donor site, lack of enough endurance of the implants, and low rate of successful transplantations.

Cartilage tissue engineering has been widely studied as a promising alternative therapy that creates biocompatible scaffolds incorporating genes, growth factors, and drugs to promote the proliferation and differentiation of chondrocytes at the injury site. An ideal articular cartilage construct could fill the defect void with tissue with the same mechanical properties as articular cartilage and enhance the integration between the repairing tissue and the native articular cartilage [61,62].

Among the biopolymers used for fabricating artificial cartilage, SF has been widely considered by researchers because of its suitable tunable properties, biodegradability, biocompatibility, low immunogenicity, and high mechanical strength quality. Cheng et al. had a Comprehensive overview of SF-based scaffolds for cartilage tissue engineering. Another systematic review was conducted by Fazel and coworkers, focusing on applying Bombyx mori SF for the regeneration of cartilage tissue [61,62].

Li and coworkers used extrusion-based low-temperature 3D printing to develop a macro-porous hydrogel scaffold through horseradish peroxidase (HRP)-mediated cross-linking of silk fibroin (SF) and tyramine-substituted gelatin (GT) (SF-GT hydrogel) (Fig.6(a)). Compared to

17

previous submicron or nano-sized gel networks, the SF-GT macro-porous structure hydrogel led to a more supply of oxygen and nutrients. It enhanced the proliferation and differentiation of encapsulated cells. As cartilage regeneration is considerably time-consuming, the scaffold degradation rate is crucial in sufficient cartilage repair [63].

As shown in Fig.6(b), increasing the SF proportion and the treatment with methanol has delayed the degradation of hydrogel scaffolds. Subsequently, stem cells were seeded on scaffolds via cell suspension and cell aggregate methods. As shown in Fig.6(c), cell aggregate seeding led to higher collagen type II expression levels and showed hyaline cartilage phenotype. An in-vivo animal study also revealed that the scaffold with CA group showed a smooth articular surface, and more tissue was regenerated (Fig.6(d)) [64].

In another study, a novel porous SF scaffold was fabricated using an enzymatic-horseradish peroxidase (HRP)-mediated approach to crosslink SF combined with salt-leaching and freeze-drying technologies cartilage regeneration applications. As presented in Fig.6(e), more intensive protein expression of chondrogenic-related markers (collagen type II, Sox-9, and Aggrecan) was observed after 28 days of culture in a chondrogenic culture differentiation medium. Compared to basal culture conditions, subcutaneous implantation of the scaffolds in CD-1 mice also indicated the adherence of a thick layer of connective tissue on the entire surface of the platforms which deeply infiltrated into the porous structures [65].

Zhang et al. developed a bio-ink composed of different concentrations of SF and decellularized ECM (SF-dECM bioinks) mixed with bone marrow mesenchymal stem cells (BMSCs) for 3D bioprinting. SF-dECM 3DBP scaffolds enhanced chondrogenesis of BMSCs by increasing the expression of SOX-9, collagen II (COL II), aggrecan (ACAN), and collagen I (COL I) mRNA, which progresses the chondrogenic differentiation process. Furthermore, they

encapsulated TGF-β3 into the construct to validate the control of the release behavior of the system, showing a sustained long-term release and inhibited burst release of TGF-β3 (Fig.7(a)). The Histological sections stained with Masson's trichrome and safranin O as well as immunohistochemical analysis of collagen II in the printed constructs after 28-days of incubation exhibited that release of TGF-β3 caused a greater intensity of staining in the SF-dECM construct loaded with TGF-β3 as compared to that without TGF-β3 (Fig.7(b)) [66].

To create a 3D porous microenvironment to attenuate inflammation and facilitate chondrogenic differentiation, Wu and colleague established SF coated gelatin porous scaffold (GSTR) loaded with ginsenoside Rb1 and TGF-β1, which induces anti-inflammatory, anti-apoptosis response and regulates chondrogenic differentiation of mesenchymal stem cells (MSCs), respectively. As demonstrated in Fig.7(c), SF-coated scaffolds (GSTR) degraded much slower than none- SF-coated scaffolds (GTR) over time and also showed a slower release of Rb1 and TGF-β1 than GTR (Fig.7(d)). Moreover, The implantation of in vivo patches into the osteochondral defects for 12 weeks showed that GSTR scaffolds effectively promote the regeneration of hyaline after surgery and create a thicker layer of tight and normal cartilage-like tissue compared with other groups (Fig.7(e)) [67].

Lately, Liu et al. incorporated Poloxamer (Pluronic F127) grafted on SF-Alginate patches to produce thermosensitive ALG-POL/SF hydrogels with covalently and physically crosslinked networks which are injectable with sol-gel transitions in physiological pH and temperature. It was unveiled that ALG-POL/SF gels have enhanced mechanical properties, and as well support the in-growth of chondrocytes while endorsing their development toward chondrogenesis tissue [68].
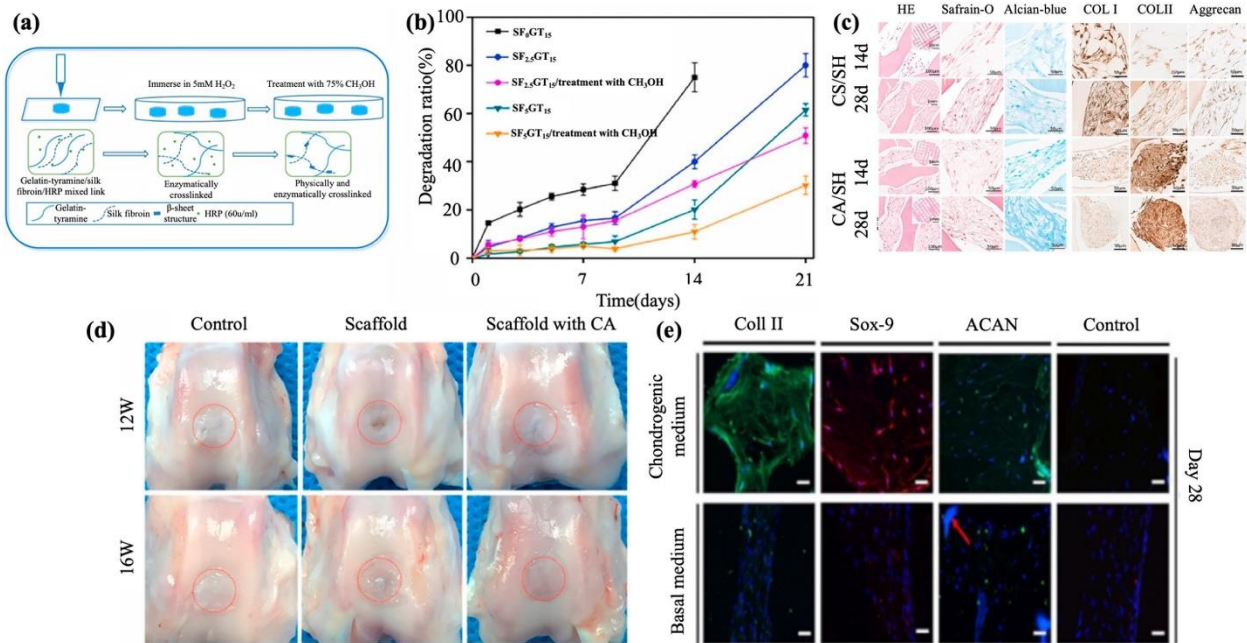
Fig.6 (a) Schematic diagrams of the 3D SF-GT hydrogel scaffold synthesis. (b) degradation of 3D printed hydrogel scaffolds. (c) Evaluation of cartilage formation of CA/SH and CS/SH cultured in chondrogenic differentiation medium. The sections were stained with H&E, safranine-o, Alicia-blue after 14 and 28 days of culture, COL I, COL II, and Aggrecan immunohistochemical staining. (d) In vivo animal tests. Harvested joints after 12 weeks and 16 weeks showing regenerated cartilage tissue [64]. (e) Immunofluorescence analysis of the chondrogenic-related markers. Nuclei are stained blue, Col II and ACAN in green, and Sox-9 in red [65].

In a study conducted by Lee and associates, a ternary hydrogel of Gellan Gum (GG), SF, and Chondroitin Sulfate (CS) were developed for cartilage tissue engineering. It was detected that GG's accumulation advances the hydrogel's mechanical properties, but a proportion percentage of GG higher than 75 % leads to a harsh gelation condition for cell encapsulation. The 0.5% GG/3.5% SF/CS group showed a higher expression of Cartilage-specific genes, leading to more effective maintenance of chondrocytes in substrate-generated phenotypes, which ought to be applied as a promising cartilage tissue engineering construct [69].
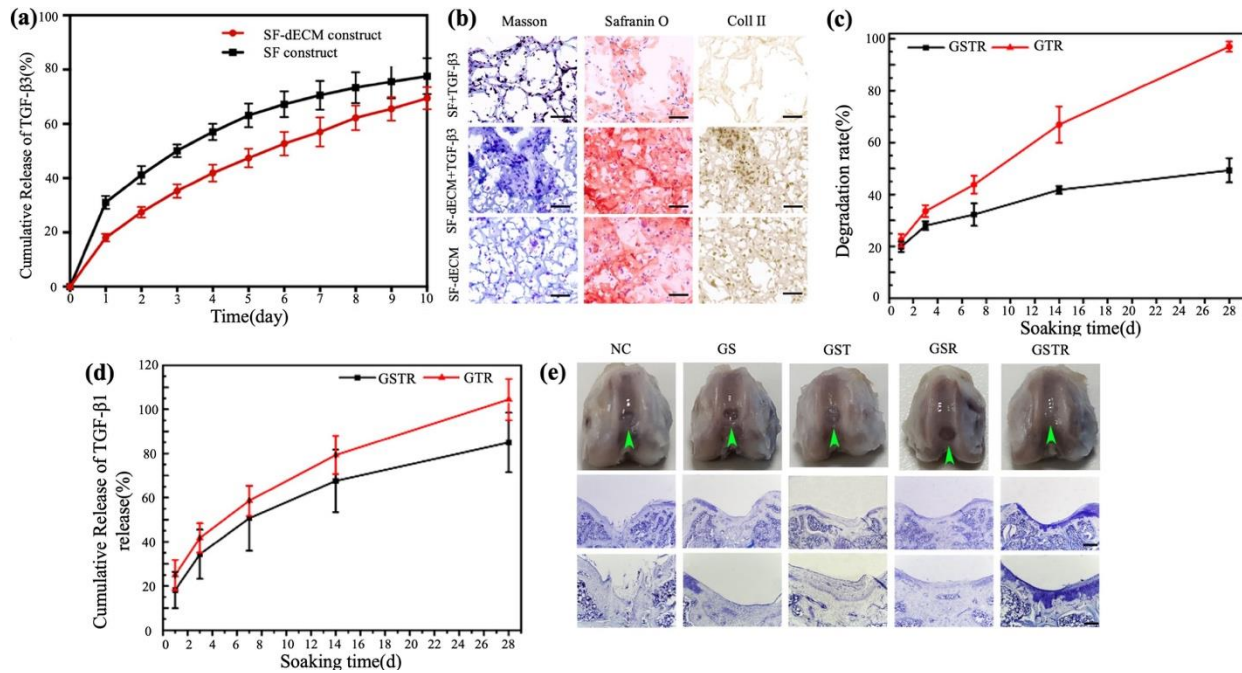
Fig.7 (a) Release of TGF-β3 from the SF-dECM construct. (b) Histological sections stained with Masson's trichrome and safranin O and immunohistochemical analysis of collagen II in the printed constructs after 28 d of incubation [66]. (c) Degradation (d) and TGF-β1 release behaviors of GTR and GSTR scaffold.(e) Histological comparison of scaffolds implanted into the defects after 12 weeks [67].

Freshly, a hybrid system of SF-hydrogel scaffolds incorporated with chitosan (CS) nanoparticles (NPs) was designed for cartilage defect regeneration application. chitosan (CS) nanoparticles (NPs) were incorporated with growth factor-β1 and SF incorporated with bone morphogenetic protein-2 (BMP-2; TGF-β1@CS/BMP-2@SF) (Fig.8(a)). The TGF-β1@CS/ BMP-2@SF group demonstrated the best repair effect compared to the control and CS/SF groups. The cartilage defect areas were filled with hyaline cartilage, BMSCs differentiated to chondrocytes, and inflammatory cell infiltration further decreased [70].

Another composite hydrogel of SF and carboxymethyl chitosan (CMCS) was settled with enzymatic cross-links (horseradish peroxidase and hydrogen peroxide) and β-sheet cross-links (ethanol treatment) (Fig.8(b)). They explored the effect of ethanol treatment period on morphology, equilibrium swelling, degradation, rheological properties, and mechanical properties. Therein, the hydrogels with 2-hours ethanol treatment showed the most proper properties for artificial cartilage. The ability of EA0 (the hydrogels with 0 h ethanol treatment) and EA2 (the hydrogels with 2 h ethanol treatment) hydrogels to maintain chondrocyte phenotype was analyzed by measuring the expression levels of cartilage related genes. It was observed that there was a higher gene expression in EA2 hydrogel than in EA0 ones, indicating that EA2 hydrogel could effectively support the chondrocyte phenotype [71].

Zhang et al. designed an injectable bone marrow mesenchymal stem cell (BMSC)-encapsulated double network hydrogel based on collagen (Col), SF, and PEG. Col and PEG were initially modified with Col-Norbornene (Nb) and Tetrazine (Tz), which crosslink to form the first network, and then ultrasonic induction was applied to trigger the formation of a second SF network. BMSCs were premixed in the precursor solutions and encapsulated in the hydrogel after gelation (Fig.8(c)). The chondrogenic differentiation analysis of BMSCs within the hydrogels demonstrated that a great expression of chondrogenic genes, including Col II and Aggrecan (AGG) (Fig.8(d, e)) which confirm the excellent potential of Col-PEG/SF DN hydrogels for the chondrogenic differentiation of BMSCs and cartilage tissue engineering [72].

Chen et al. used dehydrothermal (DHT) treatment, a low-cost, low-cytotoxicity physical crosslinking method, for developing elastin-like polypeptides (ELP) modified SF scaffolds. Elastin-like polypeptides (ELPs) improve the differentiation of BMSCs towards a chondrogenic

lineage without the addition of chondrocyte-specific growth factors and also enhance adhesion and differentiation of BMSCs and chondrocytes [73].
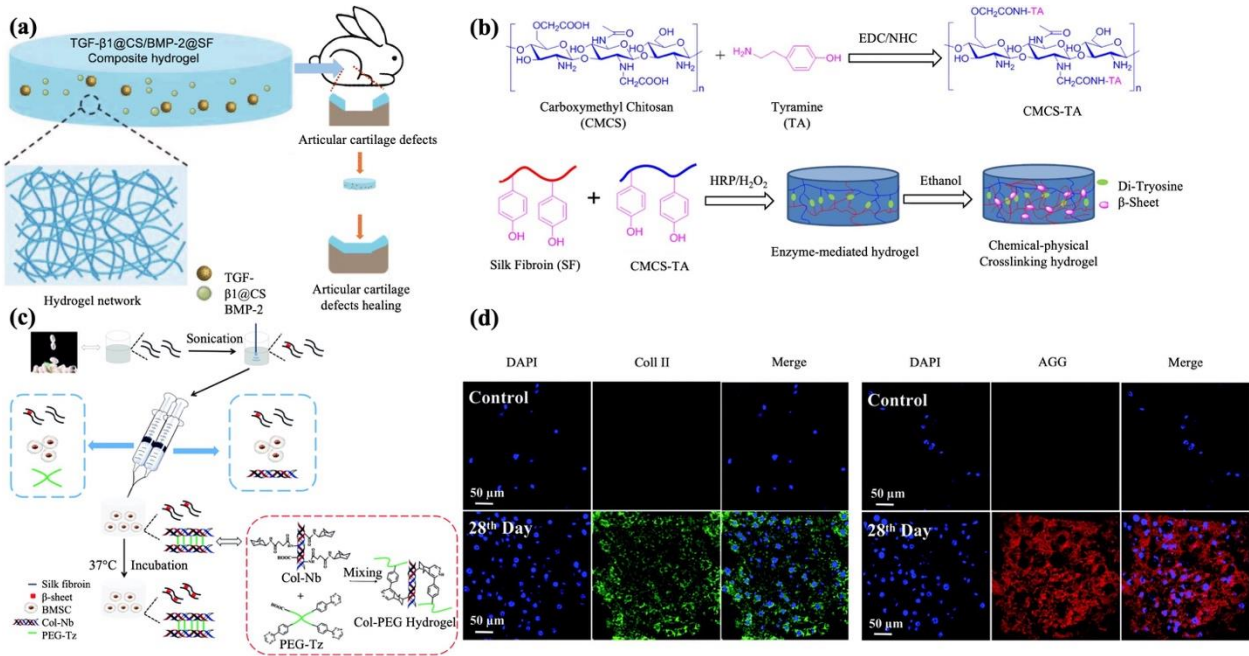
Fig.8 (a) The scheme of TGF-β1@CS/BMP-2@SF composite hydrogel [70]. (b) The scheme of hydrogel formation and characterization of CMCS-TA [71]. (c) Preparation of the BMSC-laden injectable Col-PEG/SF hydrogel for cartilage regeneration. Immunofluorescence staining of Col II (d) and AGG of the BMSC-laden Col5-PEG5/SF5 hydrogel after culturing in chondrogenic differentiation medium for 0 (control) and 28 days [72].

4. Controlled Drug Delivery

In recent years, controlled drug delivery systems (DDSs) have been extensively investigated to optimize the efficacy of therapeutics (ThP) and supply the correct dose thereof to the desired body compartment in a controlled manner [74]. DDS diminishes the dose frequency, improves patient compliance, minimizes drug concentrations fluctuation, maintains blood levels within the

therapeutic range, and reduces adverse effects on healthy tissues [75]. An ideal DDS is developed by biocompatible and biodegradable materials with non-toxic by-products and offers strong mechanical properties for controlling the burst release of the loaded drug [74]. To date, both synthetic and natural polymers have been studied and employed for drug delivery applications, among which Silk based materials are one of most favored candidates as they can blend with other polymers to enhance their chemical and biological properties [7,76]. In addition to the composition, many studies have reported remarkable advantages of nanostructured drug delivery carriers in treating human diseases by ThP target delivery [77]. The nanocarriers' small size, with large surface area to volume ratio, can readily interact with biomolecules and enter the target cells, which improves the absorption, bioavailability, stability, and ThP-controlled release [78]. Hereunder, an overview of the Silk-based nanostructured DDSs specifically for cancer treatment and wound healing (WH) applications is presented.

4.1 Silk-based DDS for Cancer therapy

Although extensive research and numerous innovative approaches are being developed for cancer treatment, the disease is lasting its trend as the second leading cause of mortality throughout the world [79]. By 2040, it's estimated that the incidence of all cancers will have risen from just over 19 million in 2020 to 30.2 million [80]. While conventional treatment methods such as surgical intervention, chemotherapy, and radiation therapy lead to the cancer cells' death, it also damages the surrounded healthy tissues and causes undesirable side effects. Overcoming these challenges, numerous delivery systems have been established delivering chemotherapeutics (Ch-ThP) to the tumor sites with enriched therapeutic efficacy and lower cytotoxicity to the enclosed tissues [81].

Natural polymers have been preferred to design an anticancer DDS over synthetic polymers due to their excellent biocompatibility and desirable pharmacokinetics, and Silk as a natural protein has been identified as a promising biopolymer for biomedical and pharmaceutical

24

applications. Furthermore, hydrophobic interaction between the SF crystallites and anticancer drugs governs the drug stabilization. Also, carboxyl and amino group availability in the SF allows bio-functionalization of various biomolecules or ligands, which can be used as targeted DD. Different SF-based DDSs are widely discussed with innovative methods generating functionalized SF systems for controlling the DD to the cancer tissues [82].

Wu et al. developed encapsulated anticancer drug Paclitaxel (PTX) into SF, without any toxic organic solvents. PTX-loaded nanoparticles (NPs) with a mean diameter of 130 nm were formed in an aqueous solution at room temperature by self-assembling SF protein, and efficiently taken by two human gastric cancer cell lines, BGC-823, and SGC-7901. In addition, the superior antitumor efficacy of PTX-loaded SF-NPs was shown to delay tumor growth and reduce the tumor weight compared with systemic administration in gastric cancer nude of mice xenograft model [83]. In 2014, a team of researchers prepared loaded SF-NPs with an average diameter of 59 nm by an electro-spraying method without using an organic solvent [84]. The in-vitro release pattern showed that loading Cis-Dichlorodiamminoplatinum (CDDP) in the SF-NPs contributes to a slow,sustained drug release over 2 weeks (Fig.9(a)). To examine the cytotoxicity effects of CDDP-loaded SF-NPs, incubation with both A549 lung cancer cells and L929 mouse fibroblast cells were done. It was detected that both non-CDDP-loaded and CDDP-loaded SF-NPs prompt apoptosis in A549 lung cancer cells, which confirms that the drug loading process did not affect the anticancer activity of the CDDP (Fig.9(b)). As shown in Fig.9(c), the CDDP-loaded SF-NPs avoided the cytotoxicity and killing effect on L929 as normal healthy cells [84].

Several studies have developed novel DDSs that respond to acidic tumor tissue's milieu to improve the efficiency of cancer treatment. It is accepted that the cancer cells' pH is more acidic than a normal cell; therefore, pH-sensitive DDSs are promising engineered vehicles conveying the

25

cancer therapies to tumor sites with non-toxic effects affecting the healthy tissues [85]. Among pH-sensitive biomaterials, Silk, as a native biopolymer, is able to elicit drug release in response to pH without any chemical modifications [86].

In 2013, Seib et al. developed Doxorubicin (DOX)-loaded Silk NPs for breast cancer (B-C) treatment and examined the pH-dependent release and lysosomal accumulation of Silk-NPs by monitoring the DOX release behavior in buffers with pH values mimicking those of blood plasma (pH 7.4), endosomes (pH 6.0), and lysosomes (pH 4.5). As demonstrated in Fig.9(d), the drug release was significantly faster from the DOX-loaded Silk NPs in pH 4.5 than for the other pH conditions. Virtually, at lower pH values, Silk loses its acidic surface properties and has a negative net charge, reducing the electrostatic interactions between Silk and DOX, which in turn increases the drug release (Fig.9(e)). The cytotoxicity effect of DOX-loaded Silk NPs was also surveyed using human B-C cell lines. A more cytotoxic effect was perceived than the free drug at the DOX equivalent dose [86]. Wu et al. also prepared injectable pH-responsive silk hydrogels nanofibers to deliver DOX for B-C localized chemotherapy [87].
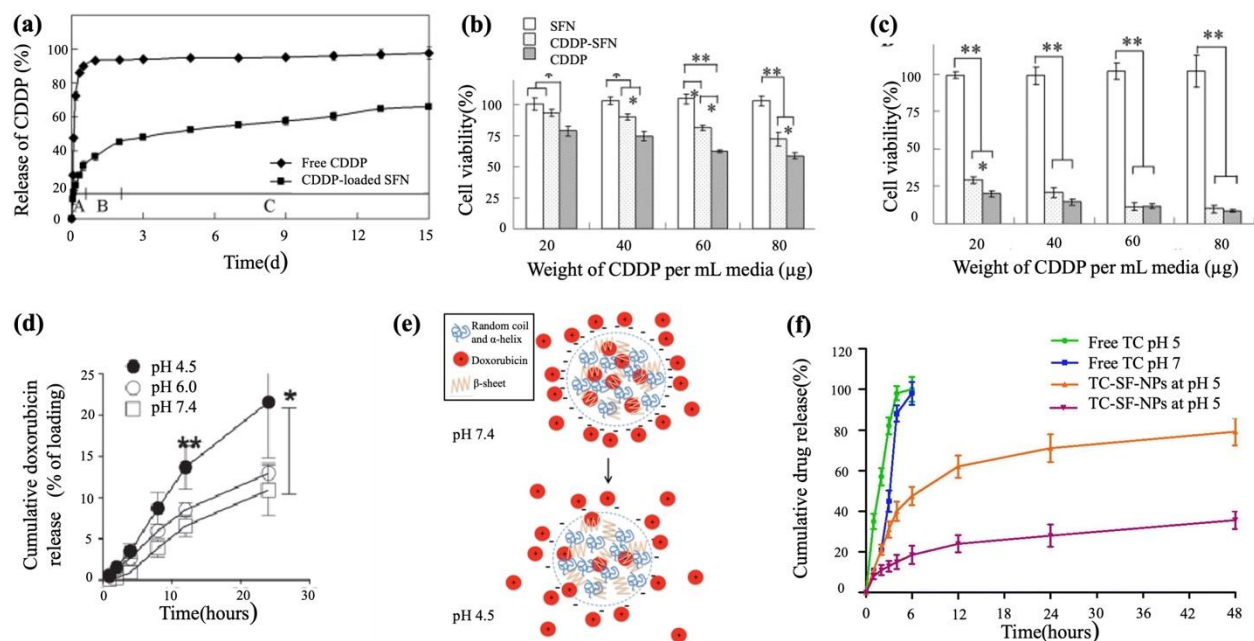
Fig.9 (a) Release of cisplatin from silk fibroin nanoparticles. (b) A549 cell viability of different cisplatin formulas after culture for 1 d.(c) L929 cell viability with varying formulas of cisplatin after culture for 1 d [84]. (d) pH-dependent release of doxorubicin during the first 24 h and subsequent 6 days. (e) schematic representation of silk nanomedicines. pH-dependent release of doxorubicin from a silk nanoparticle [86]. (f) In vitro release study of free TC and TC-loaded SF-NPs at different pH. TC: tamoxifen citrate; TC-SF-NPs: tamoxifen citrate silk fibroin nanoparticles [88].

In another study, tamoxifen citrate (TC)-loaded SF-NPs with an average particle size of 186.1 ± 5.9 nm were established for B-C healing. To examine the effect of natural pH condition on the release pattern of TC from TC-loaded SF-NPs, they mimicked the physiological pH (pH 7.4) and tumor-associated pH environment (pH 5) in vitro. They witnessed that TC release was significantly faster from SF-NPs when incubated in an acidic medium (pH 5.0) rather than at pH 7.4 (Fig.9(f)). Therefore, SF-based carriers ought to act as pH-responsive DDS and control the drug release rate in low pH tumor-associated tissues. Furthermore, the apoptosis assay showed the

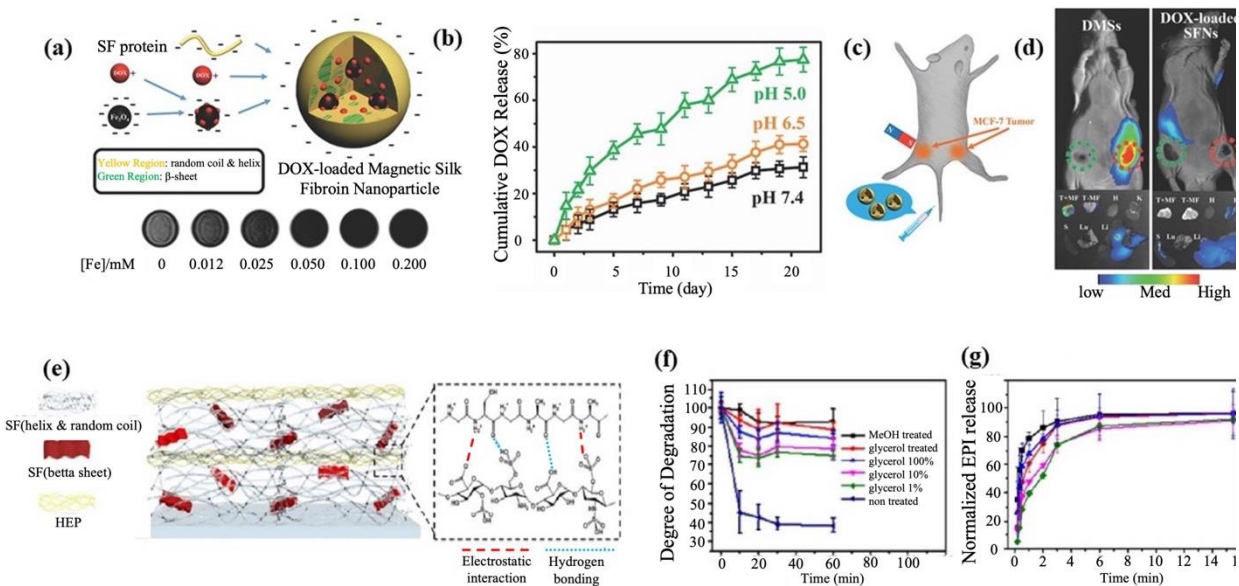remarkable cytotoxicity effects of TC-loaded SF-NPs against B-C cell lines (MCF-7 and MDA-MB-231) [88].

Fig.10 (a) Schematic illustration of the formation of DMSs. (b) pH-dependent release of DOX during 3 weeks. (c) A schematic drawing to illustrate magnetic tumor targeting. (d) Fluorescence in vivo images (bottom view) of mice bearing two MCF-7 tumors on both sides at 2-hours post-injection of DMSs or DOX-loaded SFNs with an equivalent DOX dosage. Red and green circles point out tumors with and without magnet attachment, respectively [89]. (e) Schematic illustration of SF/HEP LbL-assembled nanofilms. (f) The degree of degradation (T/T$_o$) of SF/HEP LbL films depends on the added glycerol ratio and solvent treatment. (g) normalized release profile from SF/HEP LbL nanofilms [90].

Several modification methods have been leveraged to more effectively improve the native silk properties to target anticancer DD. Incorporating magnetic Fe$_3$O$_4$ NPs with Silk-based NPs has been reported to be an efficient tumor targeting method to convey Ch-ThP to the cancer site in response to an external magnetic field (MF). Compared to ligand-receptor bindings targeting,

magnetic targeting does not require chemical modification on the surface of carriers and could be easily applied to different types of tumors [89].

Tian et al. prepared DOX-loaded magnetic SF-NPs leveraging the salting-out generation process, wherein DOX was adsorbed on the surface of magnetic Fe_3O_4 NPs and then capsulated in the SF-NPs (Fig.10(a)). The DOX release profiles under different pH environments were examined, and a faster release pattern was observed in lower pH conditions (Fig.10(b)). Magnetic tumor targeting of DOX-SF-NPs was explored by intravenous injection of DOX-loaded magnetic SF-NPs (DMSs) on opposite sides of mice. Where the tumors were attached to a magnet, a considerable accumulation of DMSs was detected, and the growth of tumors was significantly inhibited compared to those without magnet attachment (Fig.10(c, d)) [89]. Another research by Song and colleagues studied the fabrication of magnetic-silk/polyethyleneimine core-shell NPs as stimuli-responsive systems to deliver c-myc antisense oligodeoxynucleotides (ODNs) to B-C cells, wherein magnetic targeting meaningfully boosted the ODNs uptake efficiencies in a short time and constrained cancer cell growth [91].

Another promising approach to expand the stability of DDSs is decorating the surface of the vehicles with PEG as a process called PEGylation, which protects the delivery systems from the host's immune system and enhances therapeutic activity [92]. For instance, Kaul et al. demonstrated a sixfold augmentation in the half-life of PEGylated versus non-PEGylated NPs in tumors [93]. Totten et al. prepared DOX-loaded native and PEGylated Silk NPs and witnessed that the PEGylation process changes the acidic surface properties of Silk NPs. In low PH conditions, like tumor tissues, DOX was released more rapidly from the PEGylated Silk-NPs than the naked NPs. To imitate the lysosomal-like environment of cancer tissues, Papain, a cysteine protease enzyme,

was induced, and the PEGylated Silk-NPs revealed a shield behavior against enzymatic degradation in the first 2 hours which coordinated the burst release of drug from the system [94].

In addition to NPs systems, SF-based DDSs-nanofilms have been developed for cancer treatment. In 2018, Choi's research group prepared multilayered nanofilms via Layer-by-Layer (LbL) assembly of SF and heparin (HEP) using glycerol and methanol (MeOH) as solvents. The chemical structures of SF/HEP films and the functional groups of SF and HEP with their electrostatic interactions and hydrogen bonding are depicted in Fig.10(e). The physiological stability of the nanofilms is controlled by the content of the β-sheet, which is influenced by the concentration of glycerol or solvent treatment. It was reported that the MeOH treated SF/HEP-LbL film with the greatest β-sheet configuration was more physiologically stable with the lowest aqueous degradation rate (Fig.10(f)). Subsequently, the Epirubicin (EPI) anti-cancer drug was incorporated into the nanofilms. The in-vitro drug release patterns confirmed that a higher β-sheet structure in MeOH treated SF/HEP-LbL nanofilms provides a more sustained EPI release (Fig.10(g)). In addition, in-vitro cytotoxicity of the nanofilms against HeLa cells revealed that EPI loaded SF/HEP nanofilms with the highest β-sheet content are more effective in killing cancer cells [90].

4.2 Silk-based DDS for Wound Healing

Skin is the largest organ of our body responsible for protecting the internal organs against environmental exposure and hazardous pathogens [95]. Therefore, any skin integrity disruption resulting from injury or illness, such as diabetes, may lead to severe infection, disability, or even death [96]. Typical chronic wounds treatments such as topical delivery of antioxidant, anti-inflammatory, and antibacterial agents are insufficient for deep cutaneous wounds [97], and more advanced healing therapies are required [98]. Biological dressings and artificial grafts have been

30

considered effective platforms that correct irregular cellular pathways present in chronic wounds, enhance cell migration and proliferation, reduce inflammation, synthesize and secrete extracellular matrix proteins, and remodel the wound matrix [95].
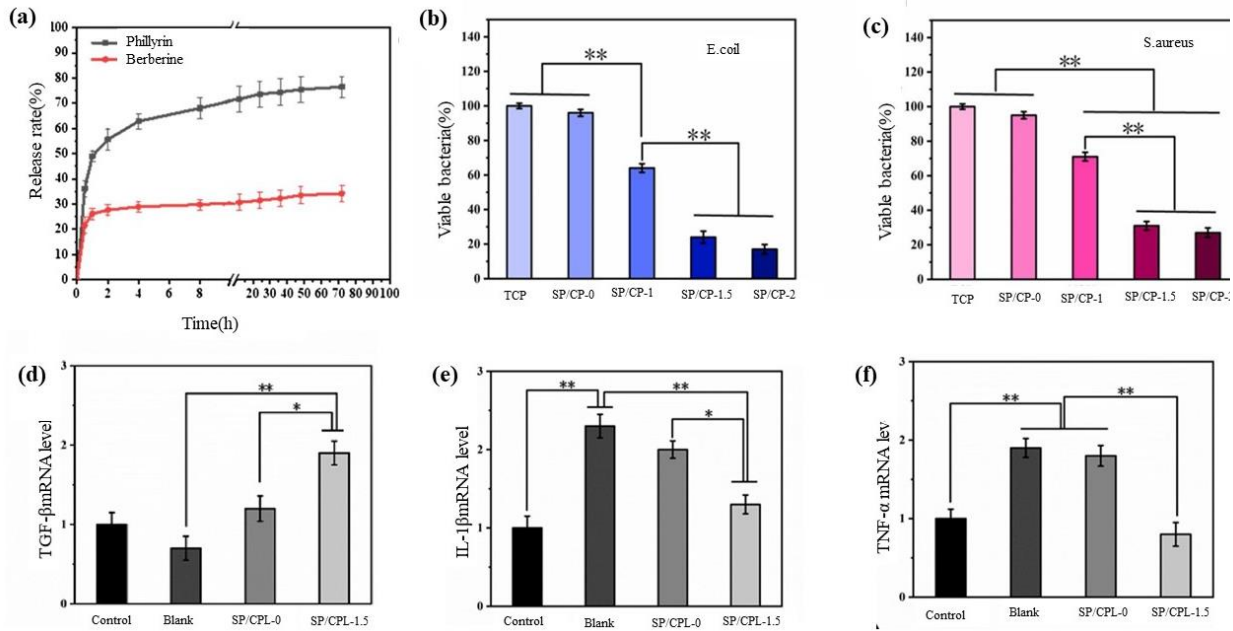

Fig.11 (a) Release behavior of Phillyrin and Berberine from SP/CPL-1.5 nanofiber membranes. (b) Statistics on the number of viable E.coli bacteria; The antibacterial results of SP/CPL nanofiber membranes (c) statistics on the number of viable S.aureus bacteria. Expression levels of genes related to wound healing on days 14. (d) TGF-β, (e) IL-1β, (f) TNF-α [99].

Among different biopolymers utilized to develop bioactive matrices in WH applications, Silk based mediums have shown great potential in treating chronic ulcers [100]. Silk proteins as biocompatible, non-immunogenic, and bioresorbable material heighten the necessary procedure of the recovery process such as cell migration, cell proliferation, angiogenesis, and re-epithelialization. Moreover, silk media could be functionalized with bioactive molecules and antimicrobial compounds to provide a sustained release of ThP into the wound bed [95]. The

functionalized Silk-based matrices could be fabricated with different platforms such as nanofibers, porous scaffolds, thin films, and hydrogels. Chouhan and coworkers have extensively discussed the silk-based functionalized DDS utilized for WH applications [95]. Herein, we overview the most recent signs of progress in Silk-based materials for cutaneous injuries treatments.
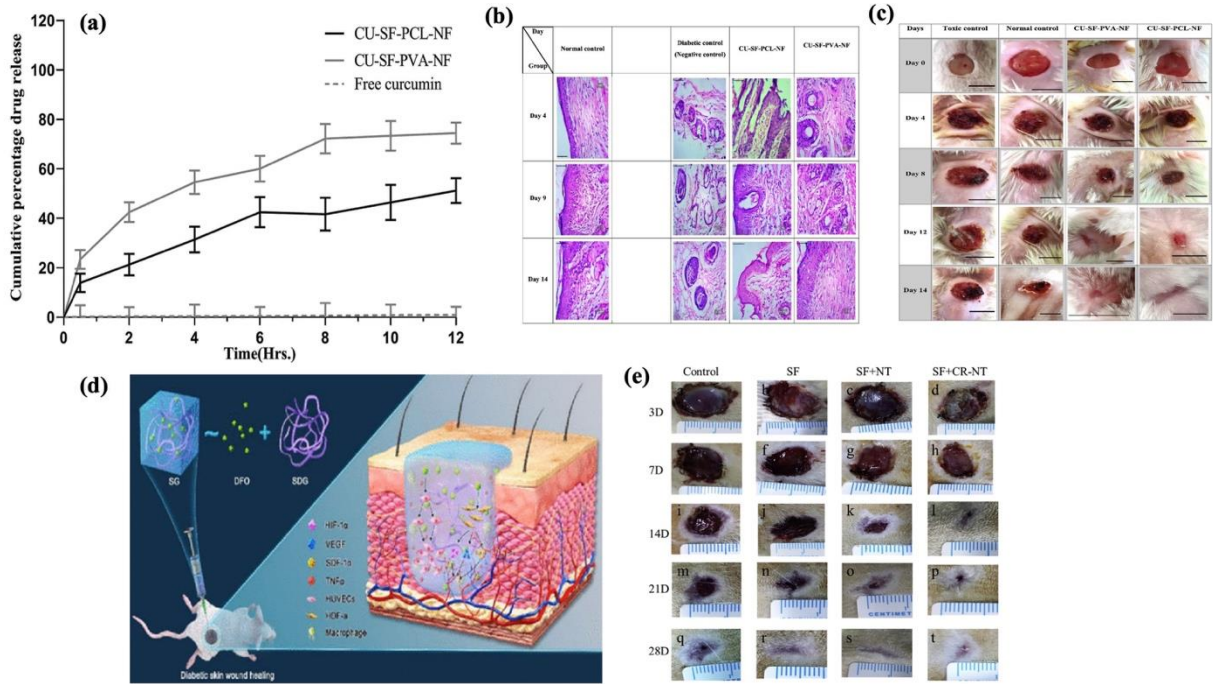
Fig.12 (a) In vitro curcumin release from optimized nanofibrous formulations and free curcumin in phosphate buffer solution pH 7.4 (mean ± SD, n = 3) (b) Histopathology of wounded skin tissue images of Normal control, Diabetic control, CU-SF-PCL-NF and CU-SF-PVA-NF (Scale bar -100μm). (c) Photographic images of wound healing in streptozotocin-induced diabetic mice after treating animals with TC (toxic control), NC (normal control), placebo,CU-SF-PCL-NF, and CU-SF-PVA-NF [101]. (d) Schematic illustration of Desferrioxamine (DFO) laden SF nanofiber (SFN) hydrogels [102]. (e) The different effects of wound healing by four procedures in diabetic rats [103].

Yerra et al. established antibiotic-based-SF (ABSF) film that targets bacterial pathogens at the site of burn wounds; it was perceived that the ABSF films, as well, promote cell adhesion and

directly contact the layer of the wound, and, by releasing the antibiotics into the attached microbial cells, target the pathogens at the wound site. Therefore, the designed ABSF films can diminish the risk of infections and accelerate the healing process [104]. In another study, SF-poly-(L-lactide-co-caprolactone) (PLCL) nanofibers were fabricated and blended with Compound Phellodendron Liquid (CPL), a promising drug for WH, to treat diabetic ulcers.

An in-vitro drug release study, showing the slow-release pattern after 2 hours (Fig.11(a)), reported through the antibacterial analysis of the SP/CPL nanofibers that the number of colonies shrank by increasing the CPL content. The antibacterial effects against gram-negative bacteria (E.coli) are more than gram-positive bacteria (S. aureus) (Fig.11(b)). In addition, as shown in Fig.11(c), the nanofibers loaded with CPL enhance the expression of TGF-β (Fig.11(d)) with a significant inhibition effect on the expression of inflammatory factors (IL-1β and TNF-α), promoting rapid WH as demonstrated in Fig.11(e, f) [99].

Agarwal et al. prepared SF-curcumin-based nanofiber blended with polycaprolactone (PCL) and polyvinyl alcohol (PVA) to improve the physicochemical properties of the SF nanofibers for the diabetic wound treatment. The in-vitro curcumin release from developed nanofibers showed a biphasic drug release pattern leading to primary burst release for the first hour and following sustained release, which induced a more extended therapeutic response. It was also observed that the Curcumin-loaded SF-PVA showed a faster release compared to nanofiber prepared with SF-PCL (Fig.12(a)). Moreover, both histopathological studies (Fig.9(b)) and in-vivo WH efficacy analysis in diabetic induced mice showed that the maturation and remodeling stage of WH get almost complete on day 14 for CU-SF-PCL, and CU-SF-PVA nanofiber treated groups with the WH rate of 99% and 96.54%, respectively (Fig.12(c)) [101].

In another study, Desferrioxamine (DFO) laden SF nanofiber (SFN) hydrogels were fabricated to treat diabetic foot ulcers (Fig.12(d)). The DFO was discharged slowly from the hydrogels over 40 days, providing a sustained therapeutic delivery to chronic wounds, and the DFO-laden SFN hydrogels modulated endothelial cells and macrophages, enhanced angiogenesis, reduced inflammation, and increased collagen deposition, leading to faster diabetic ulcer healing [102]. In an akin study, SF dressings with gelatin microspheres (GMs) were developed to persistently deliver neurotensin (NT) to improve diabetic foot WH. The in-vivo WH processes in the rat diabetic model demonstrated that the wound almost fully cured in NT/GMs/SF group within 28 days (Fig.12(e)). They also indicated that The NT/GMs/SF dressings stimulated fibroblast accumulation and collagen deposition at the wound site leading to a faster ulcers healing [103].

In a recent study, a heparin-immobilized fibroin hydrogel loading FGF1 (human acidic fibroblast growth factor 1) was prepared and carried out to cover cutaneous defects on the back of rats. The in-vivo WH efficacy study showed that the heparinization process decreases the time required to achieve total wound closure by faster re-epithelization and earlier granulation tissue formation [105].

5. Wearable Bioelectronics and Biosensors

Nowadays, the galloping rate at which intelligent textiles, wearable sensors, flexible displays, and medical equipment are flourishing requires designing mechanical-sensitive, flexible, and biodegradable devices. Biosensors are based on signals transduced by various mechanisms and categorized into electrochemical, calorimetric, piezoelectric, and optical biosensors [106] which can be applied in different ways; some are wearable, implantable, or ingestible [107]. SF as a biodegradable natural polymer has the potential to be used in all these categories [108]. Due to Silk's inherent piezoelectricity [109], harvesting energy from human motions and potentially using it as wearable and self-powered sensors are among those applications [110].

34

In order to promote the piezoelectric properties of smart materials, using composition synthesizing approaches is a conventional strategy [111], whoever controlling the morphology of the fabricated scaffolds has been considered also [112]. In addition to them, some groups have recently triggered the microstructural evolution effect on piezoelectric properties of the electro active biomaterials [113]. To begin with, a team has developed a pressure sensor made of thin silk film with d_{33} values close to PVDF's value [114]. It was also illustrated that electrospun Silk fiber has good piezoelectric properties ($d_{33} \approx 38 \pm 2$ pm/V) even after stabilization with methanol vapor (28 ± 3 pm/V) [115], which is applicable in bone tissue engineering approaches [116]. Bon et al. synthesized two thin films; one consisted of hot-pressed Silk on PHBV, while the other one was hot-pressed silk-gold nanorods on PHBV. Fig.13(a) displays open-circuit voltage signals of RS/PHBV and RS-GNR/PHBV, demonstrating that RS-GNR/PHBV has a more significant output signal than RS/PHBV. As discussed previously, silk piezoelectricity is dependent on the content and orientation of β-sheets. As such, piezoelectricity increases not only because of β-sheets content but also the polarization of in-plane oriented β-sheet, and can be used in electronics based on PHBV substrate [117].

Recently, Wang et al. has used core-shell electrospinning to fabricate SF/PVDF flexible piezoelectric nanofibers [118]. The coaxial structure can be verified by distinct contrast differences, as illustrated in the published transmission electron microscopy (TEM) image. This prototype has high deformation adaptability and mechanical sensitivity, assembling a suitable self-powered sensor for motion monitoring and was attached to the metacarpophalangeal joint to monitor different bending angles of the palm in time. Altered sensor amplitude observed by accumulative bending angle resulted in a positive correlation of piezoelectric voltage to the tensile strain

(Fig.13(b)). The durability of the SF/PVDF device is evaluated by a cyclic fatigue test (Fig.13(d));

it is stable even after 2000 cycles and can be efficiently applied as a sensitive strain sensor [118].
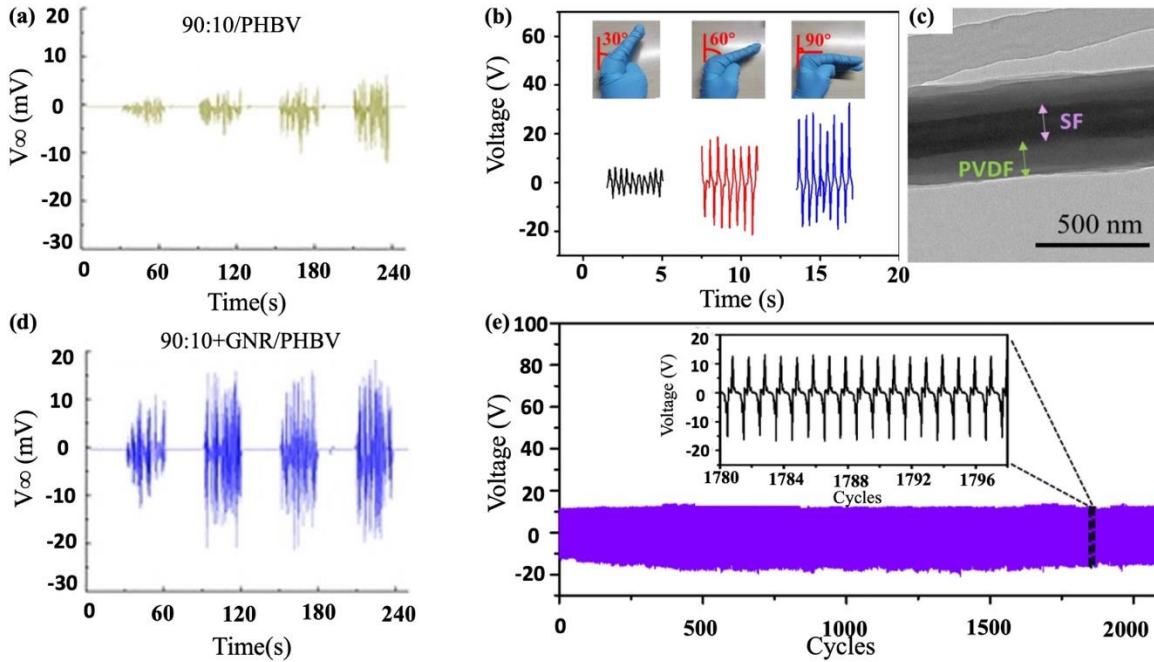

Fig.13 (a) The generated output voltage of piezoelectric devices fabricated with PHBV and RS-GNR/PHBV films,

subjected to repetitive loading and releasing pressure (frequency 1 Hz) [117]. (b) The sensor attached on the hand

bending at various angles and the corresponding piezoelectric responses. (c) TEM image of SF/PVDF nanofibers

(d, e) Durability of the SF/PVDF-14 piezoelectric device under 2 Hz and 5 mm [118].

6. Conclusion

The superior performance of Silk Fibroin in tissue engineering applications owing to its

capability for property tuning unlike conventional natural polymers points to a paradigm shift in

the design of advanced scaffolds. Adjusting mechanical/physical/chemical/biological properties

of Silk electrospun nanofibrous scaffold are yet to be investigated, and challenges related to the

fundamental issues have emerged, such as insufficient cell attachment and proliferation, wherein

the deployment of electro-sprayed particles into fibrous scaffolds could significantly promote cell

attachment and proliferation.

Considering the bending/compositing possibility, although exceedingly high number of polymers are available to be blended with SF so as to boost any property one cares to mention, only a few may prove useful, which calls for efficient high-throughput methods to modify limited useful blended nanofibers' performance.

In turn, this has led to the recent developments of fabrication techniques, compositing methods, and physiochemical treatments that not only would break through current issues and significantly enhance biological, mechanical, and chemical characteristics but also pave the path to broadening silk application. Additionally, the porous fibrous scaffold provides more surface roughness and thus a more fabulous culture medium. Designing a scaffold that can better mimic the aimed organ would significantly enhance the stand efficiency. Despite these recent advancements, the approach to reach the exact tissue mimetic scaffold with a controllable degradation rate must be further investigated.

In spite of these challenges, the SF was found to have a novel inherent feature, i.e. piezoelectricity, which ultimately led to new applications. For instance, Silk as bio-piezoelectric material generates voltage and provides electrical stimulation without electrodes or an external power source, due to discovered body's bioelectric signals. Promoted cell growth could be achieved by using bio-piezoelectric silk scaffold in tissue engineering application, where cell attachment and proliferation are in great demand. Regarding the recovery of damaged hard or soft tissue, a piezoelectric framework can give a vital incentive for cell regrowth and reduce the need for other growth factors. To boost the piezoelectric-properties of the Silk, any kind of processing which may cause a promotion in a non-centrosymmetric structure is potentially useful, which seems as an interesting field of future research.

The outstanding piezoelectricity, biodegradability, and mechanical tunabality of silk make it an excellent choice for bio-sensors applications involving wearing, implantable, and degradable devices. In view of these promising findings, we envision that more desirable silk patches with promising properties can be discovered with further advancements, thereby promoting the previously limited applications of natural polymers in biomedical applications. Considering the effects of piezoelectricity on the body, piezoelectric materials can be used to support disease recovery as well.

To reduce the dose and adverse effects of the drug on healthy tissues, DDSs are considered as an effective method in which the silk natural bio-polymer is examined for its ability to combine with other polymers and nanoparticles. For instance, the anti-cancer drug CDDP and PTX in the SF-NP system achieve anti-tumor effectiveness and reduce tumor growth. Additionally, due to the lower pH of cancer cells compared to healthy cells and silk's pH sensitivity, DDX systems are fitting options, where drug release kinetics occur steadily at low pH values.

Controlled delivery has been considered as an optimistic approach to deliver the therapeutic agents to the desired body compartment, reducing the dosing frequency and minimizing the toxic side effects on healthy tissues. As silk protein has shown excellent biocompatibility, controllable biodegradability, and non-immunogenicity, it has been presented as an adeptpolymeric biomaterials for developing controlled DDSs. This review paper also overviewed the most recent advances of silk-based nano DDSs applied for cancer treatment, as the second leading cause of death throughout the world.

Silk usage in wound dressing applications, due to the improvement of cell migration, cell proliferation, and angiogenesis seems as a fascinating approach. Thus Silk films and ABSF antibiotics hypothetically accelerate cell adhesion and healing process by targeting pathogens as it

is described as an instance for PCL, PVA and curcumin SF system which leads to a stable and effective therapeutic response. The reduction of electrostatic interactions between silk and therapeutic representatives as well as faster drug release at low pH values render silk-based DDS as a pH-dependent controlled release system in acidic tumor microenvironments.

Moreover, functionalized silk-based materials have been introduced as an excellent choice for wound healing applications due to promoting the necessary procedures of the recovery such as cell migration, cell proliferation, angiogenesis, and re-epithelialization. Overall, further investigation of SF applications in tissue engineering and drug delivery could contribute to emerging means of chronic disease treatments. Furthermore, by blending hydrophobic polymers with SF, it is possible to reduce the contact angle of the scaffold, that leads to better cell attachment and growth. The addition of bioactive agents also boosts electrical conductivity, leading to lower fiber diameters. These features make it suitable to be used in CTE.

To sum up, the reported unique characteristics of SF nominate it for numerous fruitful applications, should updated fabrication methods and compositing are utilized. Leveraging exceptional properties of this FDA-approved biopolymer towards widespread TE application would be further materialized with extensive delineation and detailed explorations of its unique merits with scientific attempts akin to what presented herein.

7. References

[1]   L. Shang, Y. Yu, Y. Liu, Z. Chen, T. Kong, Y. Zhao, *ACS Nano* **2019**, *13*, 2749.

[2]   Z. Jiao, Y. Song, Y. Jin, C. Zhang, D. Peng, Z. Chen, P. Chang, S. C. Kundu, G. Wang, Z. Wang, L. Wang, *Macromol. Biosci.* **2017**, *17*, 1.

[3]   P. Aramwit, S. Kanokpanont, W. De-Eknamkul, T. Srichana, *J. Biosci. Bioeng.* **2009**, *107*, 556.

[4]   S. Pina, I. K. Kwon, R. L. Reis, J. M. Oliveira, In *Innovative Bioceramics in Translational Medicine I: Fundamental Research* (Eds.: Choi, A. H.; Ben-Nissan, B.), Springer Singapore, Singapore, **2022**, pp. 319–350.

[5]   G. Rivero, M. D. Popov Pereira da Cunha, P. C. Caracciolo, G. A. Abraham, In *Tissue Engineering Using Ceramics and Polymers (Third Edition)* (Eds.: Boccaccini, A. R.; Ma, P. X.; Liverani, L.), Woodhead Publishing, **2022**, pp. 645–681.

[6]   P. Gupta, B. B. Mandal, In *Vascular Tissue Engineering: Methods and Protocols* (Eds.: Zhao, F.; Leong, K. W.), Springer US, New York, NY, **2022**, pp. 125–139.

[7]   T. P. Nguyen, Q. V. Nguyen, V. Nguyen, T. Le, Q. Van Le, *Polymers (Basel).* **2019**, *11*, 1.

[8]   T. Yucel, M. L. Lovett, D. L. Kaplan, *J. Control. Release* **2014**, *190*, 381.

[9]   M. A. Tomeh, R. Hadianamrei, X. Zhao, *Pharmaceutics* **2019**, *11*, 1.

[10]   V. Pandey, T. Haider, P. Jain, P. N. Gupta, V. Soni, *J. Drug Deliv. Sci. Technol.* **2020**, *55*.

[11]   A. Farahani, A. Zarei-hanzaki, H. R. Abedi, L. Tayebi, **2021**, 1.

[12]   A. Farahani, A. Zarei-Hanzaki, H. R. Abedi, I. Haririan, M. Akrami, Z. Aalipour, L. Tayebi, *J. Mater. Res. Technol.* **2021**.

[13]   S. Grabska-zielińska, A. Sionkowska, *Materials (Basel).* **2021**, *14*.

[14]   W. Sun, D. A. Gregory, M. A. Tomeh, X. Zhao, *Int. J. Mol. Sci.* **2021**, *22*, 1.

[15]   J. Pérez-Rigueiro, C. Viney, J. Llorca, M. Elices, *J. Appl. Polym. Sci.* **2000**, *75*, 1270.

[16]   A. Z. Siavashani, J. Mohammadi, M. Rottmar, B. Senturk, J. Nourmohammadi, B. Sadeghi, L. Huber, K. Maniura-Weber, *Int. J. Biol. Macromol.* **2020**, *153*, 317.

[17]   D. N. Rockwood, R. C. Preda, T. Yücel, X. Wang, M. L. Lovett, D. L. Kaplan, *Nat. Protoc.* **2011**, *6*, 1612.

[18] Y. Qi, H. Wang, K. Wei, Y. Yang, R. Y. Zheng, I. S. Kim, K. Q. Zhang, *Int. J. Mol. Sci.* **2017**, *18*.

[19] S. P. Gido, *Macromolecules* **1996**, *29*, 8606.

[20] fukada1956.pdf, .

[21] T. Yucel, P. Cebe, D. L. Kaplan, *Adv. Funct. Mater.* **2011**, *21*, 779.

[22] J. C. Lee, I. W. Suh, C. H. Park, C. S. Kim, *J. Tissue Eng. Regen. Med.* **2021**.

[23] C. Lujerdean, G.-M. Baci, A.-A. Cucu, D. S. Dezmirean, *Insects* **2022**, *13*.

[24] D. Umuhoza, F. Yang, D. Long, Z. Hao, J. Dai, A. Zhao, *ACS Biomater. Sci. Eng.* **2020**, *6*, 1290.

[25] S. Khademolqorani, H. Tavanai, I. S. Chronakis, A. Boisen, F. Ajalloueian, *Mater. Sci. Eng. C* **2021**, *122*, 111867.

[26] M. Mohammadi, M. Rajabi, M. Ghadiri, *Process. Appl. Ceram.* **2021**, *15*, 319.

[27] R. E. Unger, M. Wolf, K. Peters, A. Motta, C. Migliaresi, C. J. Kirkpatrick, *Biomaterials* **2004**, *25*, 1069.

[28] J. Rnjak-Kovacina, L. S. Wray, K. A. Burke, T. Torregrosa, J. M. Golinski, W. Huang, D. L. Kaplan, *ACS Biomater. Sci. Eng.* **2015**, *1*, 260.

[29] Y. Sang, M. Li, J. Liu, Y. Yao, Z. Ding, L. Wang, L. Xiao, Q. Lu, X. Fu, D. L. Kaplan, *ACS Appl. Mater. Interfaces* **2018**, *10*, 9290.

[30] J. Liu, T. Li, H. Zhang, W. Zhao, L. Qu, S. Chen, S. Wu, *Mater. Today Bio* **2022**, *14*, 100243.

[31] W. Kim, H. Lee, C. K. Lee, J. W. Kyung, S. B. An, I.-B. Han, G. H. Kim, *Adv. Funct. Mater. n/a*, 2105170.

[32] Z. Mao, X. Bi, F. Ye, P. Du, X. Shu, L. Sun, J. Guan, X. Li, S. Wu, *Int. J. Biol.*

41

Macromol. **2021**, *182*, 1268.

[33] Y. Song, H. Wang, F. Yue, Q. Lv, B. Cai, N. Dong, Z. Wang, L. Wang, *Adv. Healthc. Mater.* **2020**, *9*, 1.

[34] C. Patra, S. Talukdar, T. Novoyatleva, S. R. Velagala, C. Mühlfeld, B. Kundu, S. C. Kundu, F. B. Engel, *Biomaterials* **2012**, *33*, 2673.

[35] C. Yan, Y. Ren, X. Sun, L. Jin, X. Liu, H. Chen, K. Wang, M. Yu, Y. Zhao, *J. Photochem. Photobiol. B Biol.* **2020**, *202*, 111680.

[36] H. Nazari, E. Esmaeili, A. M. Gorabi, **2020**, 248.

[37] Y. Liu, J. Lu, G. Xu, J. Wei, Z. Zhang, X. Li, *Mater. Sci. Eng. C* **2016**, *69*, 865.

[38] Y. Liang, A. Mitriashkin, T. Ting, J. C. Goh, *Biomaterials* **2021**, *276*, 121008.

[39] X. Zhang, C. B. Baughman, D. L. Kaplan, *Biomaterials* **2008**, *29*, 2217.

[40] F. P. Seib, M. Herklotz, K. A. Burke, M. F. Maitz, C. Werner, D. L. Kaplan, *Biomaterials* **2014**, *35*, 83.

[41] H. Liu, X. Li, G. Zhou, H. Fan, Y. Fan, *Biomaterials* **2011**, *32*, 3784.

[42] Q. Liu, G. Ying, N. Jiang, A. K. Yetisen, D. Yao, X. Xie, Y. Fan, H. Liu, *Med. Nov. Technol. Devices* **2021**, *9*, 100051.

[43] L. Yu, X. F. Hao, Q. Li, C. C. Shi, Y. K. Feng, *Adv. Mater. Res.* **2014**, *1015*, 336.

[44] D. Kochhar, M. K. DeBari, R. D. Abbott, *Front. Bioeng. Biotechnol.* **2021**, *9*, 1.

[45] A. Leal-Egaña, T. Scheibel, *J. Mater. Chem.* **2012**, *22*, 14330.

[46] J. Song, Z. Chen, L. L. Murillo, D. Tang, C. Meng, X. Zhong, T. Wang, J. Li, *Int. J. Biol. Macromol.* **2021**, *166*, 1111.

[47] T. Wu, J. Zhang, Y. Wang, D. Li, B. Sun, H. El-Hamshary, M. Yin, X. Mo, *Mater. Sci. Eng. C* **2018**, *82*, 121.

[48] X. Liu, B. Chen, Y. Li, Y. Kong, M. Gao, L. Z. Zhang, N. Gu, *J. Bioact. Compat. Polym.* **2021**, *36*, 59.

[49] H. Y. Cheung, K. T. Lau, X. M. Tao, D. Hui, *Compos. Part B Eng.* **2008**, *39*, 1026.

[50] G. B. Yin, Y. Z. Zhang, S. D. Wang, D. B. Shi, Z. H. Dong, W. G. Fu, *J. Biomed. Mater. Res. - Part A* **2010**, *93*, 158.

[51] K. Zhang, H. Wang, C. Huang, Y. Su, X. Mo, Y. Ikada, *J. Biomed. Mater. Res. - Part A* **2010**, *93*, 984.

[52] S. U. D. Wani, S. P. Gautam, Z. L. Qadrie, H. V. Gangadharappa, *Int. J. Biol. Macromol.* **2020**, *163*, 2145.

[53] W. Luangbudnark, J. Viyoch, W. Laupattarakasem, P. Surakunprapha, P. Laupattarakasem, *Sci. World J.* **2012**, *2012*.

[54] C. Lei, H. Zhu, J. Li, J. Li, X. Feng, J. Chen, *Polym. Eng. Sci.* **2015**, *55*, 907.

[55] A. Keirouz, M. Zakharova, J. Kwon, C. Robert, V. Koutsos, A. Callanan, X. Chen, G. Fortunato, N. Radacsi, *Mater. Sci. Eng. C* **2020**, *112*, 110939.

[56] C. Acharya, S. K. Ghosh, S. C. Kundu, *Acta Biomater.* **2009**, *5*, 429.

[57] C. M. Srivastava, R. Purwar, A. P. Gupta, *Int. J. Biol. Macromol.* **2019**, *130*, 437.

[58] S. Bin Bae, M. H. Kim, W. H. Park, *Polym. Degrad. Stab.* **2020**, *179*, 109304.

[59] S. S. Shera, R. M. Banik, *J. Bionic Eng.* **2021**, *18*, 103.

[60] A. J. Sophia Fox, A. Bedi, S. A. Rodeo, *Sports Health* **2009**, *1*, 461.

[61] G. Cheng, Z. Davoudi, X. Xing, X. Yu, X. Cheng, Z. Li, H. Deng, Q. Wang, *ACS Biomater. Sci. Eng.* **2018**, *4*, 2704.

[62] M. Farokhi, F. Mottaghitalab, Y. Fatahi, M. Reza, **2019**, *115*, 251.

[63] R. S. Tuan, A. F. Chen, B. A. Klatt, *J. Am. Acad. Orthop. Surg.* **2013**, *21*, 303.

[64]   Q. Li, S. Xu, Q. Feng, Q. Dai, L. Yao, Y. Zhang, H. Gao, H. Dong, D. Chen, X. Cao, *Bioact. Mater.* **2021**, *6*, 3396.

[65]   V. P. Ribeiro, S. Morais, F. R. Maia, R. F. Canadas, J. B. Costa, A. L. Oliveira, J. M. Oliveira, R. L. Reis, *Acta Biomater.* **2018**.

[66]   X. Zhang, Y. Liu, C. Luo, C. Zhai, Z. Li, Y. Zhang, T. Yuan, *Mater. Sci. Eng. C* **2021**, *118*, 111388.

[67]   T. Wu, Y. Chen, W. Liu, K. L. Tong, C. W. W. Suen, S. Huang, H. Hou, G. She, H. Zhang, X. Zheng, J. Li, Z. Zha, *Mater. Sci. Eng. C* **2020**, *111*.

[68]   J. Liu, Q. Fang, H. Lin, X. Yu, H. Zheng, Y. Wan, *Carbohydr. Polym.* **2020**, *247*, 116593.

[69]   S. Lee, J. Choi, J. Youn, Y. Lee, W. Kim, S. Choe, J. Song, R. L. Reis, G. Khang, *Biomolecules* **2021**, *11*.

[70]   Y. Li, Y. Liu, Q. Guo, **2021**, 1.

[71]   T. Li, X. Song, C. Weng, X. Wang, L. Gu, X. Gong, Q. Wei, X. Duan, L. Yang, C. Chen, *Int. J. Biol. Macromol.* **2019**, *137*, 382.

[72]   Y. Zhang, M. Liu, R. Pei, *Mater. Adv.* **2021**, *2*, 4733.

[73]   Z. Chen, Q. Zhang, H. Li, Q. Wei, X. Zhao, F. Chen, *Bioact. Mater.* **2021**, *6*, 589.

[74]   D. Bhowmik, H. Gopinath, B. P. Kumar, S. Duraivel, K. P. S. Kumar, **2012**, *1*, 24.

[75]   K. Park, *J. Control. Release* **2014**, *190*, 3.

[76]   B. Tyler, D. Gullotti, A. Mangraviti, T. Utsuki, H. Brem, *Adv. Drug Deliv. Rev.* **2016**, *107*, 163.

[77]   J. K. Patra, G. Das, L. F. Fraceto, E. V. R. Campos, M. D. P. Rodriguez-Torres, L. S. Acosta-Torres, L. A. Diaz-Torres, R. Grillo, M. K. Swamy, S. Sharma, S. Habtemariam, H. S. Shin, *J. Nanobiotechnology* **2018**, *16*, 1.

[78]   Z. Hami, *Ann. Mil. Heal. Sci. Res.* **2021**, *19*, 1.

[79]   H. Nagai, Y. H. Kim, *J. Thorac. Dis.* **2017**, *9*, 448.

[80]   H. Sung, J. Ferlay, R. L. Siegel, M. Laversanne, I. Soerjomataram, A. Jemal, F. Bray, **2021**, *71*, 209.

[81]   Y. Dang, J. Guan, *Smart Mater. Med.* **2020**, *1*, 10.

[82]   B. Crivelli, S. Perteghella, E. Bari, M. Sorrenti, G. Tripodo, T. Chlapanidas, M. L. Torre, *Soft Matter* **2018**, *14*, 546.

[83]   P. Wu, Q. Liu, R. Li, J. Wang, X. Zhen, G. Yue, H. Wang, F. Cui, F. Wu, M. Yang, X. Qian, L. Yu, X. Jiang, B. Liu, *ACS Appl. Mater. Interfaces* **2013**, *5*, 12638.

[84]   J. Qu, Y. Liu, Y. Yu, J. Li, J. Luo, M. Li, *Mater. Sci. Eng. C* **2014**, *44*, 166.

[85]   J. Liu, Y. Huang, A. Kumar, A. Tan, S. Jin, A. Mozhi, X. Liang, *Biotechnol. Adv.* **2013**.

[86]   F. P. Seib, G. T. Jones, J. Rnjak-kovacina, Y. Lin, D. L. Kaplan, **2013**.

[87]   H. Wu, S. Liu, L. Xiao, X. Dong, Q. Lu, D. L. Kaplan, *ACS Appl. Mater. Interfaces* **2016**, *8*, 17118.

[88]   A. Moin, S. Ud, D. Wani, R. A. Osmani, A. S. A. Lila, S. Khafagy, H. H. Arab, H. V Gangadharappa, N. Ahmed, *Drug Deliv.* **2021**, *28*, 1626.

[89]   Y. Tian, X. Jiang, X. Chen, Z. Shao, W. Yang, *Adv. Mater.* **2014**, *26*, 7393.

[90]   M. Choi, D. Choi, J. Hong, *Biomacromolecules* **2018**, *19*, 3096.

[91]   W. Song, D. A. Gregory, H. Al-janabi, M. Muthana, Z. Cai, *Int. J. Pharm.* **2019**, *555*, 322.

[92]   J. J. F. Verhoef, T. J. Anchordoquy, *Drug Deliv. Transl. Res.* **2013**, *3*, 499.

[93]   G. Kaul, M. Amiji, **2005**, *22*.

[94]   J. D. Totten, T. Wongpinyochit, F. P. Seib, *J. Drug Target.* **2017**, *0*, 1.

[95]   S. Regeneration, D. Chouhan, B. B. Mandal, B. B. Mandal, **2019**.

[96]   B. Of, W. Healing, **1999**.

[97]   S. Ghalei, H. Handa, *Mater. Today Chem.* **2022**, *23*, 100673.

[98]   S. C. Rizzi, K. Bott, **2010**, 143.

[99]   X. Xu, X. Wang, C. Qin, R. Khan, W. Zhang, X. Mo, *Colloids Surfaces B Biointerfaces* **2021**, *199*, 111557.

[100] P. Kamalathevan, **2018**.

[101] Y. Agarwal, P. S. Rajinikanth, S. Ranjan, U. Tiwari, J. Balasubramnaiam, P. Pandey, D. Kumar, S. Anand, P. Deepak, *Int. J. Biol. Macromol.* **2021**, *176*, 376.

[102] Z. Ding, Y. Zhang, P. Guo, T. Duan, W. Cheng, Y. Guo, X. Zheng, G. Lu, Q. Lu, D. L. Kaplan, *ACS Biomater. Sci. Eng.* **2021**, *7*, 1147.

[103] J. Liu, L. Yan, W. Yang, Y. Lan, Q. Zhu, H. Xu, C. Zheng, *Bioact. Mater.* **2019**, *4*, 151.

[104] A. Yerra, D. M. Mamatha, *Polym. Adv. Technol.* **2021**, *32*, 861.

[105] S. He, D. Shi, Z. Han, Z. Dong, Y. Xie, F. Zhang, W. Zeng, Q. Yi, *Biomed. Eng. Online* **2019**, *18*, 1.

[106] N. J. Prakash, P. P. Mane, S. M. George, B. Kandasubramanian, *ACS Biomater. Sci. Eng.* **2021**, *7*, 2015.

[107] D.-L. Wen, D.-H. Sun, P. Huang, W. Huang, M. Su, Y. Wang, M.-D. Han, B. Kim, J. Brugger, H.-X. Zhang, X.-S. Zhang, *Microsystems Nanoeng.* **2021**, *7*, 35.

[108] Q. Niu, H. Wei, B. S. Hsiao, Y. Zhang, *Nano Energy* **2022**, *96*, 107101.

[109] L. Sarkar, B. P. Yelagala, S. G. Singh, S. R. K. Vanjari, *Int. J. Energy Res.* **2022**, *46*, 3443.

[110] N. Ashammakhi, A. L. Hernandez, B. D. Unluturk, S. A. Quintero, N. R. de Barros, E. Hoque Apu, A. Bin Shams, S. Ostrovidov, J. Li, C. Contag, A. S. Gomes, M. Holgado,

Adv. Funct. Mater. n/a, 2104149.

[111] R. V Chernozem, K. N. Romanyuk, I. Grubova, P. V Chernozem, M. A. Surmeneva, Y. R. Mukhortova, M. Wilhelm, T. Ludwig, S. Mathur, A. L. Kholkin, E. Neyts, B. Parakhonskiy, A. G. Skirtach, R. A. Surmenev, *Nano Energy* **2021**, *89*, 106473.

[112] P. Bhattacharjee, B. Kundu, D. Naskar, H.-W. Kim, T. K. Maiti, D. Bhattacharya, S. C. Kundu, *Acta Biomater.* **2017**, *63*, 1.

[113] G. R. Plaza, J. Pérez-Rigueiro, C. Riekel, G. B. Perea, F. Agulló-Rueda, M. Burghammer, G. V Guinea, M. Elices, *Soft Matter* **2012**, *8*, 6015.

[114] J. Joseph, S. G. Singh, S. R. K. Vanjari, *IEEE Sens. J.* **2017**, *17*, 8306.

[115] V. Sencadas, C. Garvey, S. Mudie, J. J. K. Kirkensgaard, G. Gouadec, S. Hauser, *Nano Energy* **2019**, *66*, 104106.

[116] A. Samadi, M. A. Salati, A. Safari, M. Jouyandeh, M. Barani, N. P. S. Chauhan, E. G. Golab, P. Zarrintaj, S. Kar, F. Seidi, A. Hejna, M. R. Saeb, *J. Biomater. Sci. Polym. Ed.* **2022**, *0*, 1.

[117] S. Bittolo Bon, L. Valentini, M. Degli Esposti, D. Morselli, P. Fabbri, V. Palazzi, P. Mezzanotte, L. Roselli, *J. Appl. Polym. Sci.* **2021**, *138*, 1.

[118] S. Wang, K. Shi, B. Chai, S. Qiao, Z. Huang, P. Jiang, X. Huang, *Nano Mater. Sci.* **2021**.